

AD-A043 437

HONEYWELL CORPORATE RESEARCH CENTER BLOOMINGTON MINN  
INVESTIGATION OF MATERIAL DAMAGE. (U)

FEB 77 J F READY

F/G 20/5

UNCLASSIFIED

| OF |  
ADA  
043437

AFOSR-TR-77-1001

F44620-73-C-0022

NL



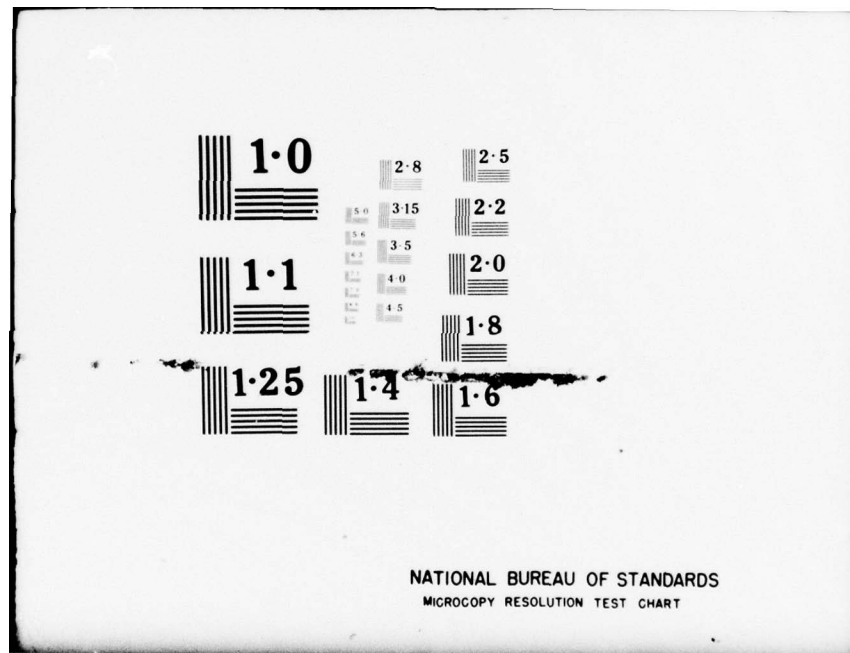
END

DATE

FILMED

9-77

DDC



**AFOSR-TR- 77 - 1001**

(12)

**AD A 043437**

**INVESTIGATION OF MATERIAL DAMAGE**

Interim Report covering period from  
15 December 1975 to 14 December 1976

by  
John F. Ready

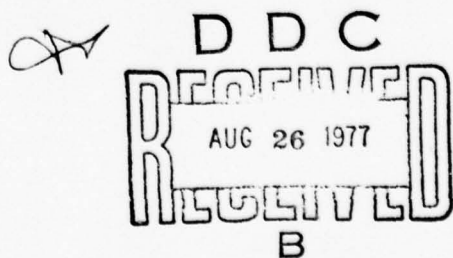
Honeywell Corporate Research Center  
10701 Lyndale Avenue South  
Bloomington, Minnesota 55420

to

Air Force Office of Scientific Research  
Directorate of Physics  
Bolling Air Force Base, Bldg. 410  
Washington, D. C. 20332

Approved for Public Release; Distribution Unlimited

**AD NO.  
DDC FILE COPY.**



AIR FORCE OFFICE OF SCIENTIFIC RESEARCH (AFSC)  
NOTICE OF TRANSMITTAL TO DDC  
This technical report has been reviewed and is  
approved for public release IAW AFR 190-12 (7b).  
Distribution is unlimited.  
A. D. BLOSE  
Technical Information Officer

(7) Interim rept. 15 Dec 75 - 14 Dec 76

**UNCLASSIFIED**

SECURITY CLASSIFICATION OF THIS PAGE (When Data Entered)

REPORT DOCUMENTATION PAGE		READ INSTRUCTIONS BEFORE COMPLETING FORM
1. REPORT NUMBER <b>AFOSR TR-77-1001</b>	2. GOVT ACCESSION NO.	3. RECIPIENT'S CATALOG NUMBER
4. TITLE (and Subtitle) <b>INVESTIGATION OF MATERIAL DAMAGE,</b>	5. TYPE OF REPORT & PERIOD COVERED Interim Dec. 15, 1975-Dec. 14, 1976	6. PERFORMING ORG. REPORT NUMBER
7. AUTHOR(s) <b>John F. Ready</b>	8. CONTRACT OR GRANT NUMBER(s) <b>F44620-73-C-0022</b>	
9. PERFORMING ORGANIZATION NAME AND ADDRESS Honeywell Corporate Research Center 10701 Lyndale Avenue South Bloomington, Minnesota 55420	10. PROGRAM ELEMENT, PROJECT, TASK AREA & WORK UNIT NUMBERS <b>16 9767-04 61102F</b>	
11. CONTROLLING OFFICE NAME AND ADDRESS Air Force Office of Scientific Research <b>NP</b> Directorate of Physics Bolling Air Force Base, Bldg. 410, Wash.D.C.	12. REPORT DATE <b>11 Feb. 1977</b>	13. NUMBER OF PAGES <b>49 1254 p.</b>
14. MONITORING AGENCY NAME & ADDRESS (if different from Controlling Office)	15. SECURITY CLASS. (of this report) <b>UNCLASSIFIED</b>	15a. DECLASSIFICATION DOWNGRADING SCHEDULE
16. DISTRIBUTION STATEMENT (of this Report)  Approved for Public Release; Distribution Unlimited		
17. DISTRIBUTION STATEMENT (of the abstract entered in Block 20, if different from Report)		
18. SUPPLEMENTARY NOTES		
19. KEY WORDS (Continue on reverse side if necessary and identify by block number) Lasers Material Damage TEA Lasers	Laser Interaction with Materials Reflectivity	
20. ABSTRACT (Continue on reverse side if necessary and identify by block number)  This report describes work performed in a continuing program of investigations on the mechanisms by which high power pulsed CO <sub>2</sub> laser radiation interacts with target surfaces. The experimental work has been performed using a pulsed CO <sub>2</sub> TEA laser capable of delivering up to 10 <sup>12</sup> w/cm <sup>2</sup> to the target surface in a pulse of duration around 100 nanoseconds. Results described in this report include the following:  <i>over 407493</i>		

UNCLASSIFIED

SECURITY CLASSIFICATION OF THIS PAGE(When Data Entered)

75% TO THE 8TH POWER

1

50 CM

1. Measurement of the pressure pulse induced in target materials by the laser pulse. Measurements were obtained as a function of target material, thickness, ambient air pressure, laser power density, and interpulse time. For metals, a typical value of peak shock pressure is around 100 bars at a laser power density around  $1.5 \times 10^8$  w/cm<sup>2</sup> at 1 atmosphere ambient pressure. For alkali halides, the results can be related to material damage.
2. Characterization of the target surface, by Auger spectroscopy and by measurements of surface scattering to determine the spectral density function.
3. Determination of the fraction of laser energy coupled into the blowoff material as a function of laser power density.
4. Construction of apparatus to determine total reflectivity as a function of time during the laser interaction.

UNCLASSIFIED

SECURITY CLASSIFICATION OF THIS PAGE(When Data Entered)

## TABLE OF CONTENTS

<u>Section</u>		<u>Page</u>
I.	INTRODUCTION AND BACKGROUND	1
II.	MEASUREMENT OF PRESSURE PULSES	5
III.	SURFACE CHARACTERIZATION	31
IV.	COUPLING OF LASER ENERGY TO BLOWOFF MATERIAL	40
V.	REFLECTIVITY	42
VI.	CONCLUSION AND FUTURE PLANS	47
	REFERENCES	49

ACCESSION for	
NTIS	White Section <input checked="" type="checkbox"/>
DDC	Buff Section <input type="checkbox"/>
UNANNOUNCED <input type="checkbox"/>	
JUSTIFICATION _____	
BY _____	
DISTRIBUTION/AVAILABILITY CODES	
Dist.	AVAIL. and/or SPECIAL
A	

## LIST OF ILLUSTRATIONS

<u>Figure</u>		<u>Page</u>
II-1	Apparatus for Measuring Free Surface Velocity	6
II-2	Shock Pressure vs Air Pressure (Al Target)	8
II-3	Shock Pressure vs Laser Power Density (Al Target)	10
II-4	Shock Pressure vs Focal Diameter (Al Target)	11
II-5	Shock Pressure vs Target Thickness (Al Target)	14
II-6	Shock Pressure vs Air Pressure (Ti Target)	15
II-7	Shock Pressure vs Laser Power Density (Ti Target)	16
II-8	Shock Pressure vs Interpulse Time (Ti Target)	19
II-9	Shock Pressure vs Time (KCl Target)	22
II-10	Shock Pressure vs Laser Power Density (KCl Target)	24
II-11	SEM Photograph of Threshold Damage in KCl	25
II-12	SEM Photograph of Damage in KCl	26
II-13	SEM Photograph of Details of Damage in KCl	27
III-1	Composition vs Depth (Unirradiated Steel)	32
III-2	Composition vs Depth (Steel Irradiated in Air)	33
III-3	Composition vs Depth (Steel Irradiated in Vacuum)	34
III-4	Measurement of Spectral Density Function	37
III-5	Spectral Density Function vs Spatial Frequency	38
IV-1	Laser Energy in Blowoff vs Laser Power Density	41
V-1	Reflectivity vs Interpulse Time	43

## SECTION I

### INTRODUCTION AND BACKGROUND

This report describes work performed on a continuing program of investigations of the interaction of high power pulsed CO<sub>2</sub> laser radiation with target materials. This program has as its goal to develop an understanding of the coupling of laser energy into materials. An accurate description of the physics of this interaction is necessary to evaluate applications of high power CO<sub>2</sub> lasers. In this work we have developed quantitative data on the interaction of the high power laser beam in a regime of laser parameters which previously had not been well explored. Using the quantitative measurements as a base, we have provided physical modeling of the interaction processes.

For our work we use a pulsed CO<sub>2</sub> TEA laser operating at a wavelength of 10.6 μm. The laser emits pulses with peak power up to 10 megawatts, which can lead to a power density at the target of up to  $10^9$  w/cm<sup>2</sup> in the focal spot. The pulse shape can be varied by changing the gas mix. When the gas mix is deficient in nitrogen, the output is a single spike of half width 100 nanoseconds. When nitrogen is added to the gas mix, a longer lower-power tail of duration several microseconds is present, in addition to the initial short spike. The initial spike is unchanged in amplitude and duration when nitrogen is added. Throughout this report we shall characterize measurements as being taken with "nitrogen off" or "nitrogen on" to describe these two different pulse shapes.

Work carried out in earlier portions of this program has been described in previous reports.<sup>(1,2,3)</sup> To make the present report reasonably self-contained and to show the relationship of the currently reported work to previous work, we shall briefly describe this background of previous experimental investigations. Specific measurement tasks have included:

- Measuring the impulse delivered to target materials by the focussed laser pulse. This part of the work used a linear velocity transducer to measure the motion of the entire target when it was struck by the laser. Measurements were obtained as a function of target material, ambient air pressure, target diameter and laser power density. The impulse decreases with decreasing air pressure down to about 10 torr. For pressures below 10 torr, a small residual component of impulse is still present because of target recoil from vaporized material. This value is approximately 0.4 dyne-second. At one atmosphere pressure, the quantitative value of the impulse is approximately 5-10 dyne-second. The results are interpreted successfully by a model in which the kindling of the laser-supported absorption wave above the surface is responsible for the observed impulse. Complete results of this task have been reported in a previous report<sup>(2)</sup> and in a published paper<sup>(4)</sup>.
- Measuring the reflectivity of the target surface as a function of time during irradiation. These measurements can be useful in determining coupling of the laser energy to the target. The specular reflectivity is probed by a beam from a continuous laser. The temporal variation of light specularly reflected from the area struck by the TEA laser pulse yields the time-resolved specular reflectivity. For the probing laser we used both a low power helium-neon laser and also a continuous CO<sub>2</sub> laser with wavelength controlled by an internal grating. This probing laser was tuned to a wavelength of 9.6 μm, so that filtering could be used to distinguish between probe light and light scattered out of the TEA laser beam. The temporal variation of the specular reflectivity was measured as a function of ambient air pressure.

TEA laser power density, pulse shape and accumulated number of pulses on the same area. Measurements as a function of ambient air pressure indicate that the change due to a single laser shot is smaller at higher values of the ambient air pressure, indicating the effect of the laser-supported absorption wave in shielding the target surface. Results at the two different probing laser wavelengths have been useful in distinguishing the mechanisms by which the surface reflectivity is changed. Quantitative descriptions of these results have been given in previous reports<sup>(2, 3)</sup> and in a published paper.<sup>(5)</sup>

- Measuring the ion energy spectrum in the blowoff material with a time-of-flight mass spectrometer. Previous reports have described this spectrometer and our unique method of data reduction.<sup>(1, 2)</sup> We have also presented data for the time-resolved spectrum of ions emitted from a number of different types of targets.<sup>(3)</sup> These results are important for understanding the coupling of laser energy into the blowoff material. We obtained the total energy content of the blowoff material as being a few percent of the incident laser energy.
- Measuring the pressure pulse coupled into the target.<sup>(3)</sup> In this effort we measured the dynamic response of the target surface; this yielded the details of the temporal development of the pressure pulse. This is done through interferometric measurements of the motion of the back surface of the target, using a helium-neon laser and a displacement interferometer, in which the back surface of the target forms one of the interferometer mirrors. At the end of the last report period we had measured the response of stainless steel targets, obtaining peak pressures of the order of 100 bars for laser power densities around  $3 \times 10^8$  w/cm<sup>2</sup>.<sup>(3)</sup>

In this report, we will discuss measurements which have extended and built upon these previous results. Much of this current work has been devoted to measuring pressure pulses under a variety of conditions. Thus, we will describe measuring the magnitude of the pressure pulse as a function of a number of the variable parameters of irradiation, and compare the results to a model of the physical processes which was described in a previous report<sup>(3)</sup> and which has been extended to include the variation of ambient air pressure. These measurements are described in detail in Section II.

In addition we have performed measurements to characterize the surface of the targets which are irradiated. These experiments, which involve both Auger spectroscopy and scattering measurements, are described in Section III.

Section IV presents additional analysis of the results obtained from the time-of-flight spectrometer, in order to obtain the variation of the amount of energy coupled into the blowoff material with laser power density.

In Section V, we discuss planned extension of the reflectivity work to involve measurement of time-resolved diffuse reflectivity from laser-irradiated surfaces. We shall also discuss the construction of equipment for these measurements.

## SECTION II

### MEASUREMENT OF PRESSURE PULSES

A major portion of the current effort has been devoted to measuring the pressure pulses delivered to various targets under varying conditions of laser irradiation. This work has involved measuring the pressure as a function of ambient air pressure, laser power density, laser pulse shape, and interpulse time for two successive laser pulses.

The experimental arrangement was described previously,<sup>(3)</sup> but for purposes of completeness we shall repeat the description here. The interferometric arrangement is shown in Figure II-1. The TEA laser pulse is focussed on the front surface of the target. The resulting laser-supported absorption wave produces a pressure pulse which propagates into the target as a shock front. When the shock front reaches the rear surface of the target, it is reflected. The rear surface moves in response to the reflection of the shock front. The motion is measured by determining the velocity of the fringes in the interferometer, for which the rear surface of the target serves as one of the mirrors. The rear surface is polished to a specularly reflecting finish.

The helium-neon laser is a Spectra-Physics Model 120 laser, which has an output of 5 milliwatts distributed among several longitudinal modes. Because the path differences in the two arms of the interferometer can be matched closely, it is not necessary to employ a single-frequency helium-neon laser. The detector is a United Detector Technology PIN-3D detector, a planar diffused silicon photodiode with a quoted response time of 15 nanoseconds. This small-area, high-frequency diode has a rise time limited by the carrier lifetime, because it operates as a current generator. The diverging lens,  $L_2$ , is adjusted so that one fringe of the interference pattern falls across the diode aperture to maximize the signal level. When the rear

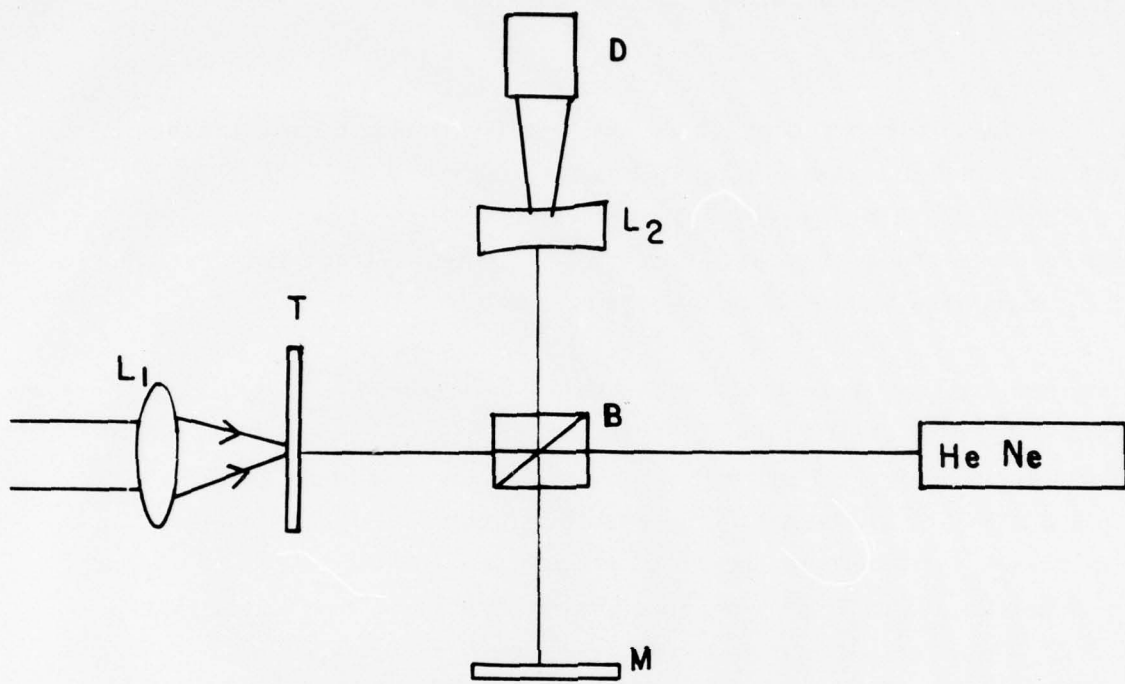


Figure II-1. Interferometric arrangement for measuring free surface velocity. The TEA laser beam is incident from the left.  $L_1$  is the lens which focuses the laser beam on the target  $T$ . The helium-neon laser beam passes through beam splitter  $B$ . The two mirrors in the Michelson interferometer are indicated as the mirror  $M$  and the rear surface of the target  $T$ . The lens  $L_2$  diverges the beam so that one fringe falls on the aperture of the detector  $D$ .

BEST AVAILABLE COPY

surface of the target moves by one-half the wavelength of the helium-neon laser light, one complete fringe in the interference pattern will move across the face of the detector, yielding an amplitude modulated output signal. The target surface velocity can be determined from the speed of the amplitude modulation of the fringes as sensed by the detector. The components are mounted on micrometer driven pedestals. This allows probing of the surface motion as a function of transverse position on the target, and also allows presentation of fresh areas for beam irradiation. The frequency response of the detector is sufficiently high to resolve the motion of the fringes produced by the target motion.

Because the interaction, propagation, and attenuation of the pressure pulse occurs in a microsecond time frame, low-frequency motion of the fringes produced by factors such as building vibration do not influence the results.

During the current report period, the apparatus was modified to allow irradiation and measurement in vacuum. In this format the target is enclosed in a bell jar. An Irtran II window admits the TEA laser beam and a glass window admits the helium-neon beam. The entire bell jar can be evacuated to a minimum pressure of  $\sim 0.01$  torr. Briefly, the measurements made as a function of ambient air pressure show, in general, that the pressure decreases with decreasing air pressure, down to approximately 10 torr. Below 10 torr, however, the pressure reaches a minimum value which does not change significantly over the range 0.01 to 10 torr.

Figure II-2 presents data from a measurement made as a function of ambient air pressure for a laser power density of approximately  $1.26 \times 10^8$  w/cm<sup>2</sup>. This illustrates the general features described above. The results are for an aluminum 2017 sample, of thickness 0.025 inch. Data are shown for two different pulse shapes, denoted nitrogen on and nitrogen off. As described in Section I nitrogen off refers to a short pulse of half width 100 nanoseconds. With nitrogen on, the initial spike is unchanged, but a longer, lower-power

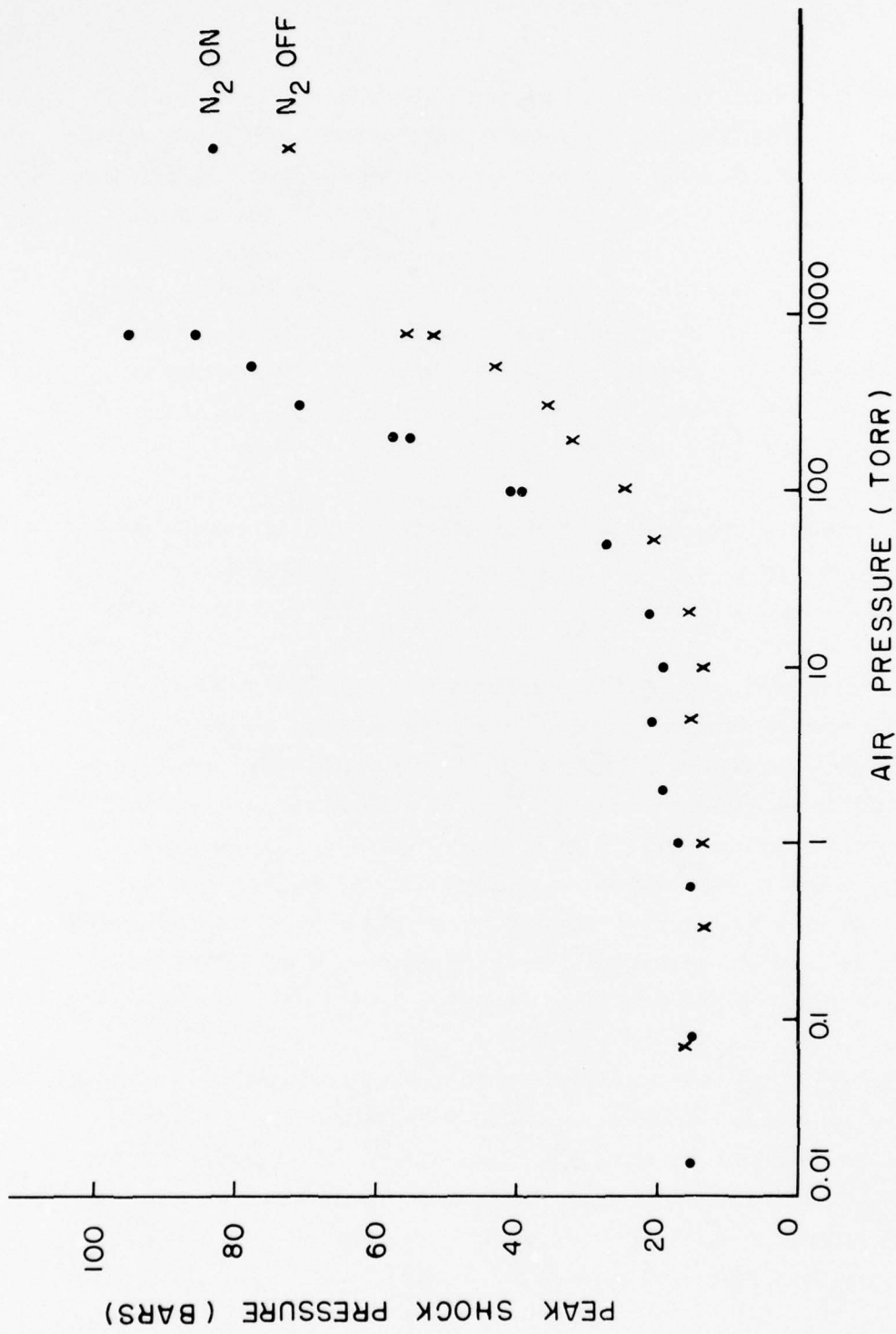


Figure II-2. Peak shock pressure as a function of ambient air pressure for an aluminum target irradiated at  $1.26 \times 10^8 \text{ w/cm}^2$ .

tail with duration of several microseconds is also present, and the energy in the pulse is increased by a factor around 3. The additional energy delivered by the tail increases the peak pressure, at least at values of air pressure above 10 torr. At 1 atmosphere pressure the increase is approximately a factor of 2. This implies that the absorption of the energy in the laser-supported absorption wave is effective in coupling a larger pressure pulse into the target material. These results are consistent with earlier results on the impulse delivered by laser pulses with these same shapes.<sup>(2)</sup> At values of ambient pressure below 10 torr, there is little difference between the two pulse shapes. The additional energy delivered at lower power is ineffective in producing increased pressure in this regime where the laser-supported absorption wave is not present.

The decrease with decreasing ambient air pressure ends near 10 torr, near the same value at which the laser-supported absorption wave has diminished. This also illustrates the role of the laser-supported absorption wave in producing the observed results.

Data on the shock pressure as a function of laser power density are given in Figure II-3, for several conditions of irradiation. The threshold near  $0.4 \times 10^8 \text{ w/cm}^2$  corresponds to the threshold for ignition of the laser-supported absorption wave. The decrease in the shock pressure as the nitrogen in the laser is turned off or as the ambient air pressure around the target is decreased is clear from these results.

In addition, data has been obtained at constant laser power but with variable laser focal diameter, by changing the distance from the focussing optics to the target. The data presented in Figure II-3 were obtained at constant focal conditions but with variable laser power. The results for variable spot diameter are shown in Figure II-4. These data were obtained in order to have available scaling relations by which the current results could be used to predict results of irradiation of larger areas, and also to compare to

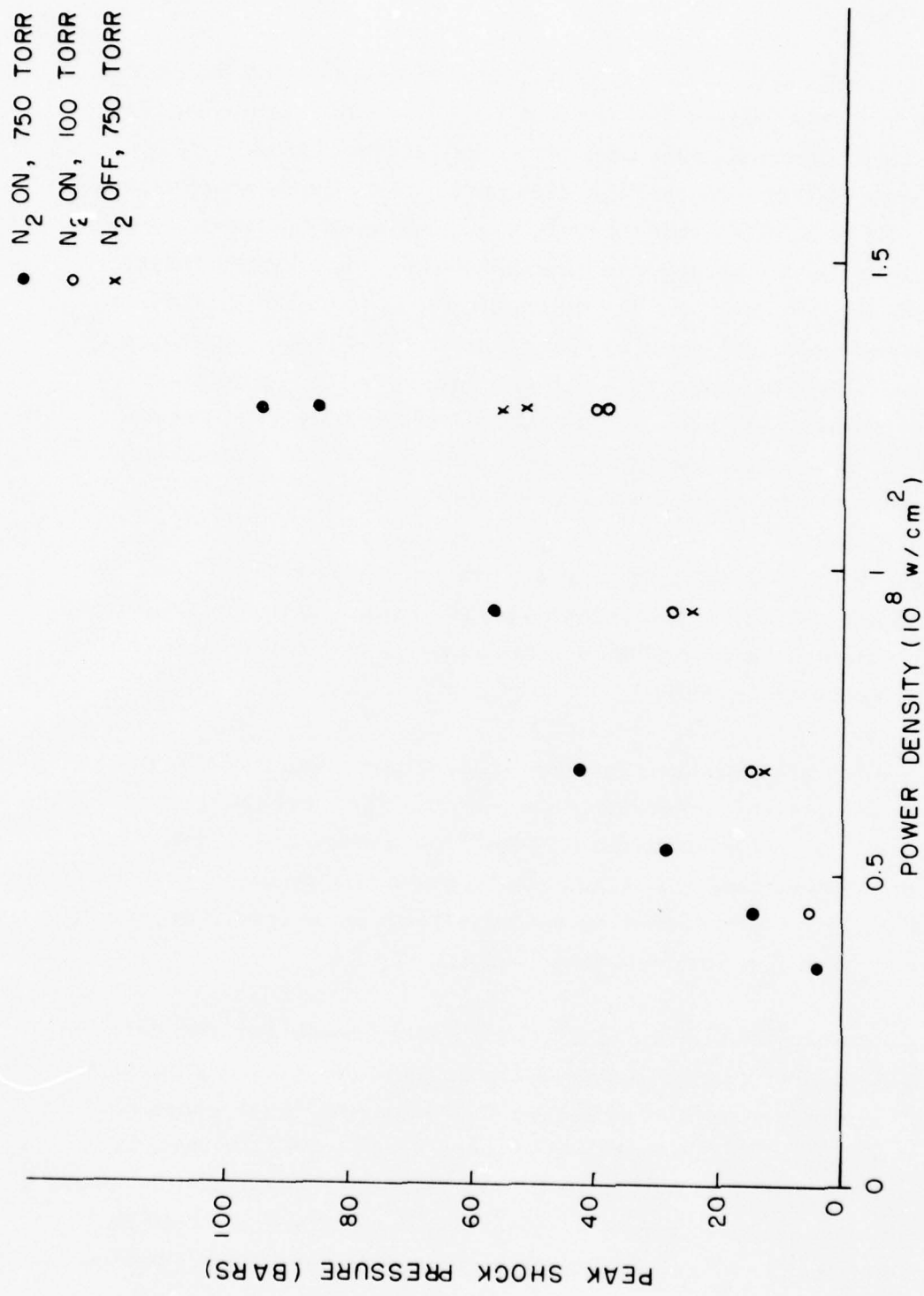


Figure II-3. Peak shock pressure as a function of laser power density for an aluminum target irradiated under the indicated conditions.

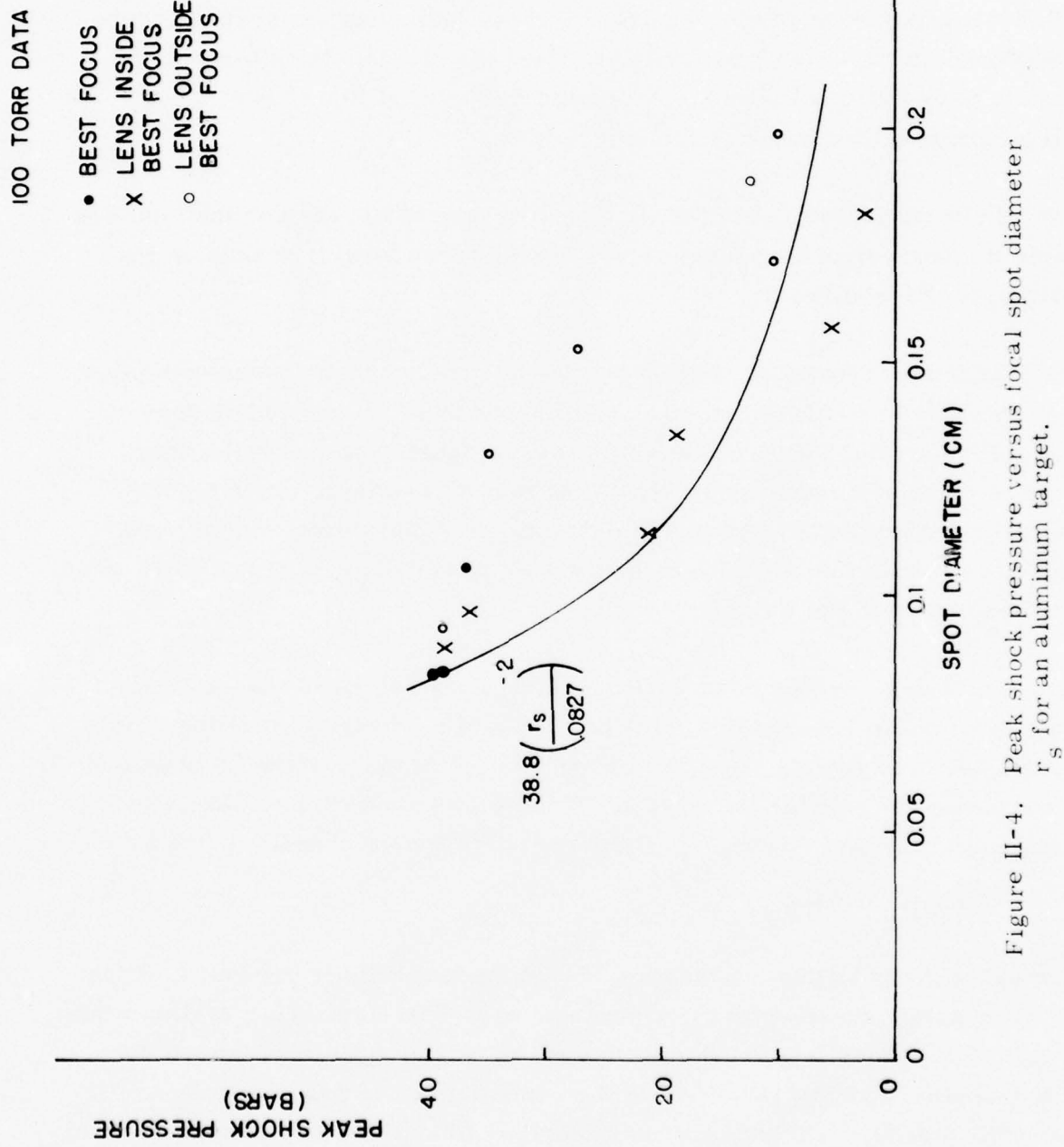


Figure II-4. Peak shock pressure versus focal spot diameter  
 $r_s$  for an aluminum target.

predictions of the physical modeling of the processes. In this figure it can be noted that the pressure decreases with increasing spot diameter and hence with decreasing laser power density. A curve indicating an inverse square dependence on the spot diameter is sketched in. The curve is normalized so as to pass through the points representing the condition of best focus. We will return to a discussion of this curve later.

It should be noted that the irradiation results depend on whether the lens lies inside the position of best focus (i. e., closer to the target) or outside the position of the best focus.

The qualitative form of this variation may be understood by considering that when the lens lies outside the position of best focus, the expanding blowoff material is moving into a region of increasing laser power density; thus, there is more absorption of energy in the blowoff and therefore a higher pressure. When the lens is inside the position of best focus, the blowoff material expands into a region of decreasing power density; hence there is less absorption in the blowoff.

We are now in a position to investigate the scaling relations, based on the data presented in Figures II-2, II-3 and II-4. The physical modeling of the process leads to scaling laws for the dependence of the peak shock pressure on the parameters of the irradiation. The development of the model was described in the last report.<sup>(3)</sup> The model yields a dependence of the form:

$$P \propto P_A^{0.61} P_o r_s^{-2}$$

where  $P$  is the peak shock pressure,  $P_A$  is the ambient air pressure,  $P_o$  is the laser power density and  $r_s$  is the focal spot diameter. This scaling would be valid for ambient air pressures in the region above 10 torr, where the laser-supported absorption wave is the dominant factor producing the observed results. A least squares power law fit to the experimental results indicates scaling as:

$$P \propto P_A^{0.51} P_0^{0.89} r_s^{-2.36}$$

This scaling holds for values of pressure above 10 torr and for laser power density above a threshold level of approximately  $0.4 \times 10^8 \text{ w/cm}^2$ . The curve showing variation with the inverse square of the focal spot diameter has already been sketched in Figure II-4, normalized to pass through the points of best focus. It fits the data obtained when the lens is inside the best focus reasonably well. Thus the model does predict results which are reasonably compatible with the experimental data. Establishing scaling laws such as these is an important part of this work, because it provides the capability of scaling our results to other conditions of laser irradiation.

To determine the effect of a finite target thickness, we measured shock pressure as a function of thickness for various aluminum targets. This was done to determine the possible attenuation of the pressure pulse that occurs as it passes through the material. Figure II-5 illustrates the results for three different thicknesses of 2017 aluminum, 0.025, 0.05 and 0.2 inches. The results show that the peak observed pressure decreases with increasing target thickness. This was expected, because of attenuation of the shock front as it passed through the material. In addition, as the target thickness becomes greater than the laser focal spot diameter, approximately 0.04 inch, the propagation of the shock front can no longer be considered one-dimensional. Attenuation through radial expansion will also occur. A linear extrapolation through the 2 points of smallest thickness indicates that at the surface the peak pressure may exceed 100 bars. If the dependence on thickness is greater than linear, the pressure at the surface will be somewhat higher.

Data for titanium alloy (4% aluminum, 4% manganese) targets 0.05-inch thick are shown in Figures II-6 and II-7. Figure II-6 shows the data for shock pressure as a function of ambient air pressure under various conditions of irradiation. The results are qualitatively similar to those obtained previously. They show a similar decrease of shock pressure with decreasing ambient air

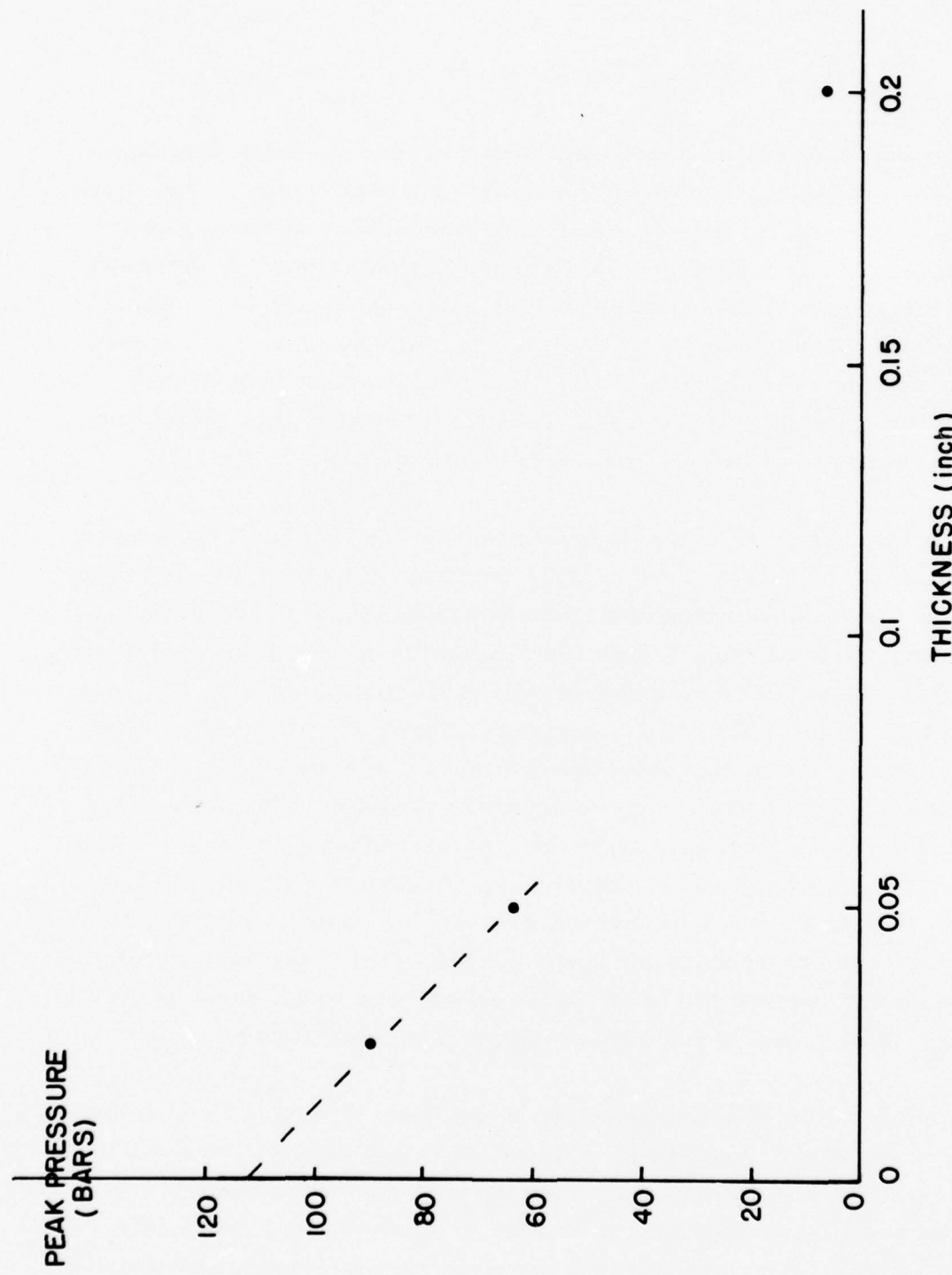


Figure II-5. Peak shock pressure as a function of target thickness for an aluminum target irradiated at  $1.16 \times 10^8 \text{ w/cm}^2$ .

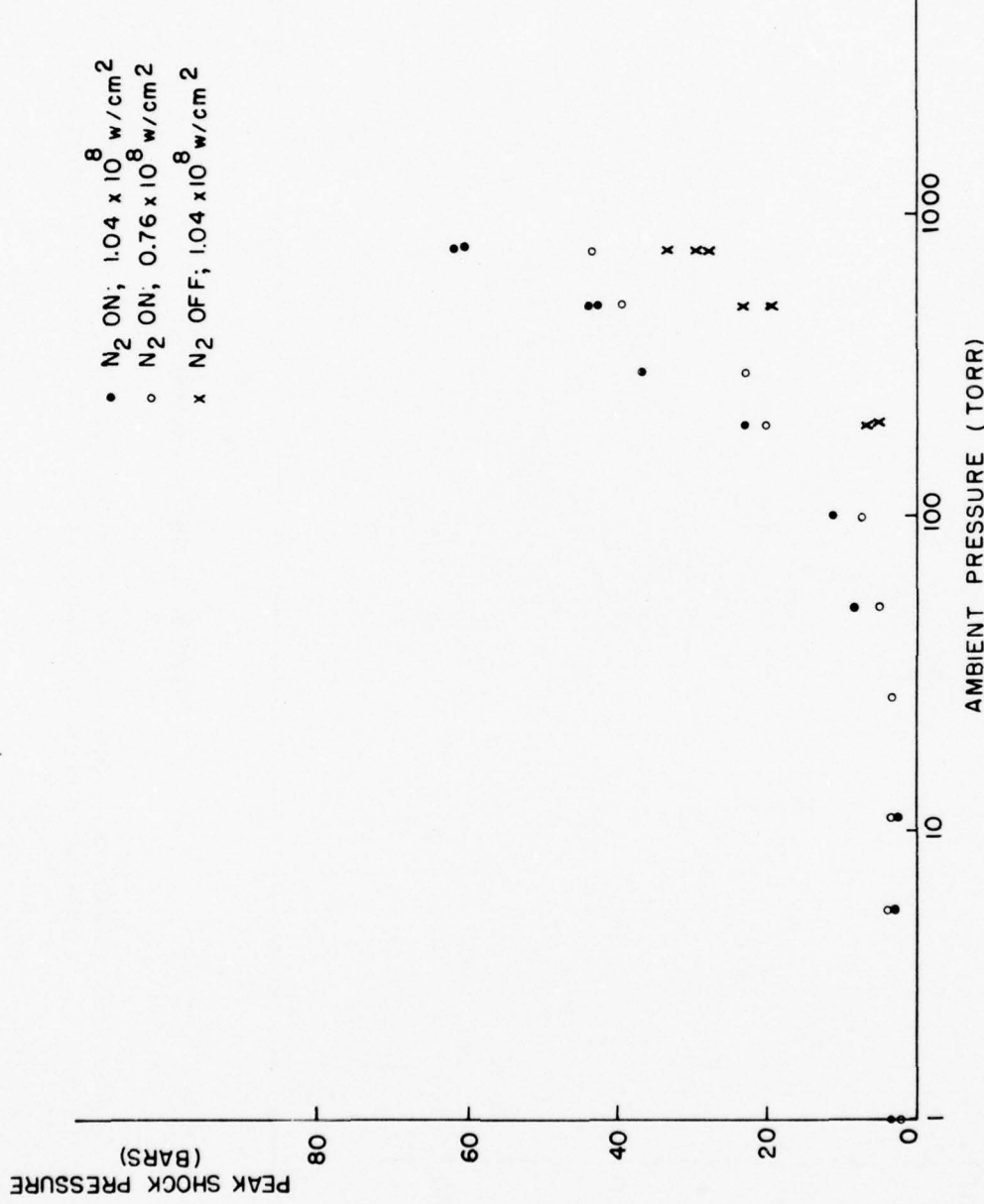


Figure II-6. Peak shock pressure versus ambient air pressure for a titanium target, irradiated under the indicated conditions.

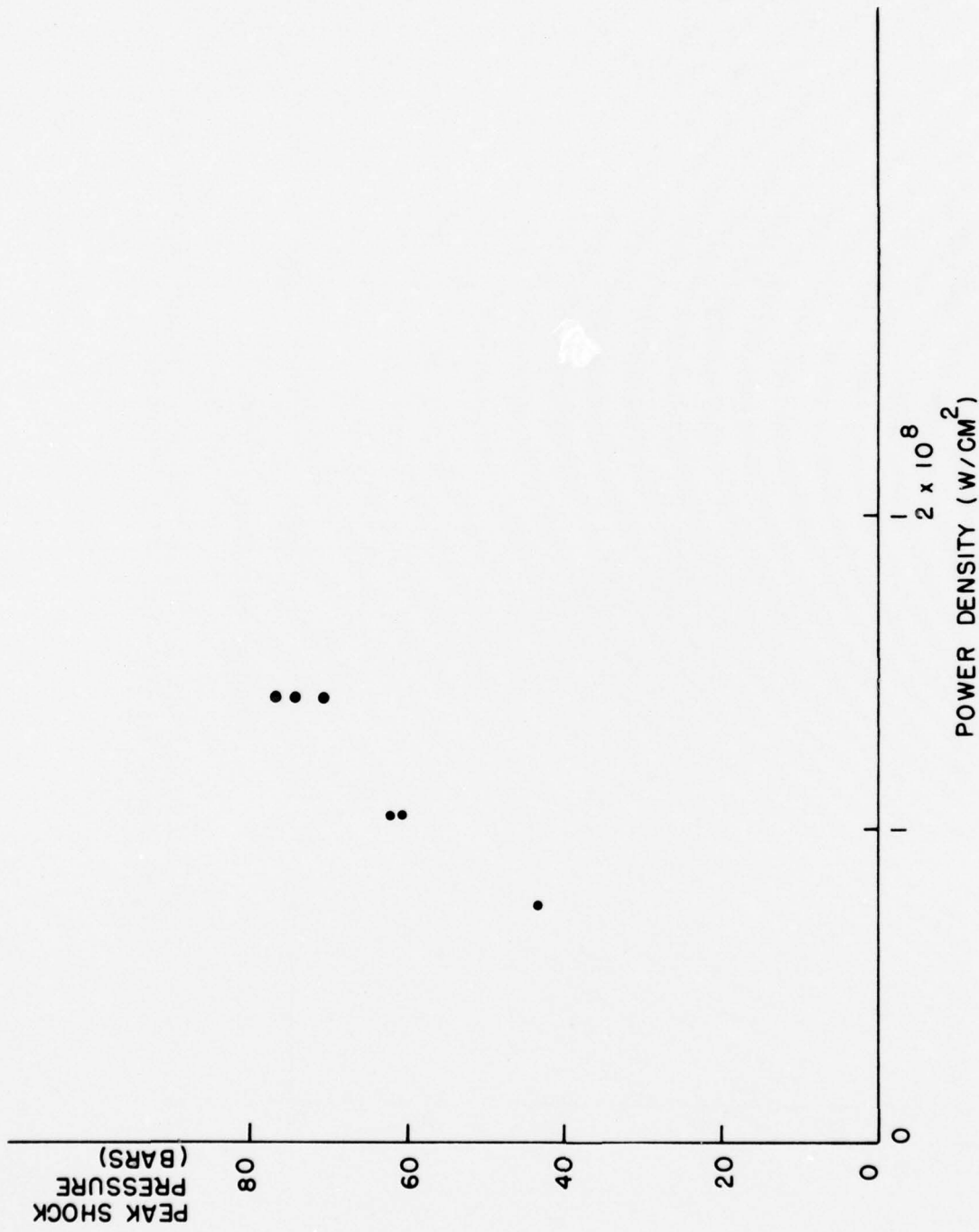


Figure II-7. Peak shock pressure as a function of laser power density for a titanium target, irradiated at 1 atmosphere ambient pressure.

pressure. The air pressure below which constant shock pressures are observed is 25 torr, somewhat higher than in the case of aluminum. In addition, the minimum value at low pressures is lower by a factor of approximately 3 than the corresponding value for aluminum. This indicates that at the indicated laser power densities, less titanium is evaporated than aluminum.

The variation of shock pressure with laser power density for the titanium target is shown in Figure II-7, for an ambient air pressure of 1 atmosphere.

To compare different materials on a consistent basis, Table II-1 presents data for all the metallic materials for which pressure has been measured, reduced to a constant value of laser power density of  $1.2 \times 10^8 \text{ w/cm}^2$ . Values had been obtained for three different thicknesses of aluminum targets as indicated. The zero thickness value is the extrapolated value as discussed above. The value for stainless steel in a 0.043-inch thick sample was derived from data presented earlier<sup>(3)</sup>. These results are all for irradiation at one atmosphere ambient pressure. We observe that the values do not vary greatly between different materials under comparable conditions of irradiation, indicating once again the dominant role of the laser-supported absorption wave in producing the shocks.

Table II-1. Values of Peak Pressure (Bars)  
 $(1.2 \times 10^8 \text{ w/cm}^2)$

Material	Thickness				
	0	0.025 in.	0.043 in.	0.050 in.	0.2 in.
Aluminum	112*	90		64	6.6
Stainless Steel			70		
Titanium				68	

\*Extrapolated

We have obtained some preliminary results on the effect of interpulse time for two successive laser pulses delivered to the same area. Figure II-8 illustrates some results for a titanium target irradiated at 1 atmosphere pressure. What is plotted is the ratio of the peak pressure produced by the second pulse to the peak pressure produced by the first pulse, in a series of two pulses. We had previously observed that the pressure produced when a second pulse was incident on a previously irradiated area did not vary significantly from the pressure produced by the first pulse, for long interpulse times.

For these data the pulse heights of the two laser pulses were monitored, to assure that the second laser pulse delivered the same power as the first. Only data satisfying this condition were accepted.

In Figure II-8, we see that for interpulse times greater than one second, the peak pressure is essentially the same for each member of a given pair of pulses. This is true to within a few percent, which is within the range of our experimental uncertainties.

For interpulse times less than one second, the peak pressure due to the second pulse becomes less than the peak pressure due to the first pulse. For an interpulse time of 140 milliseconds, the pressure due to the second pulse is reduced to about 85 percent of that due to the first pulse. This decrease continues down to the 70 millisecond regime, where the ratio is 55 percent. The minimum interpulse time that could be obtained for two equal pulses was 70 milliseconds, when these data were obtained. Only one pair of pulses could be obtained with this separation, so the exact form of the curve in this region is not certain. It does appear definite that the pressure in the second pulse continues to decrease to the lower limit of interpulse time achievable.

This lower limit was set by the stability of the laser discharge. With the available laser it was not possible to penetrate to shorter interpulse times. From the form of the data in Figure II-8, it seems that further reduction of

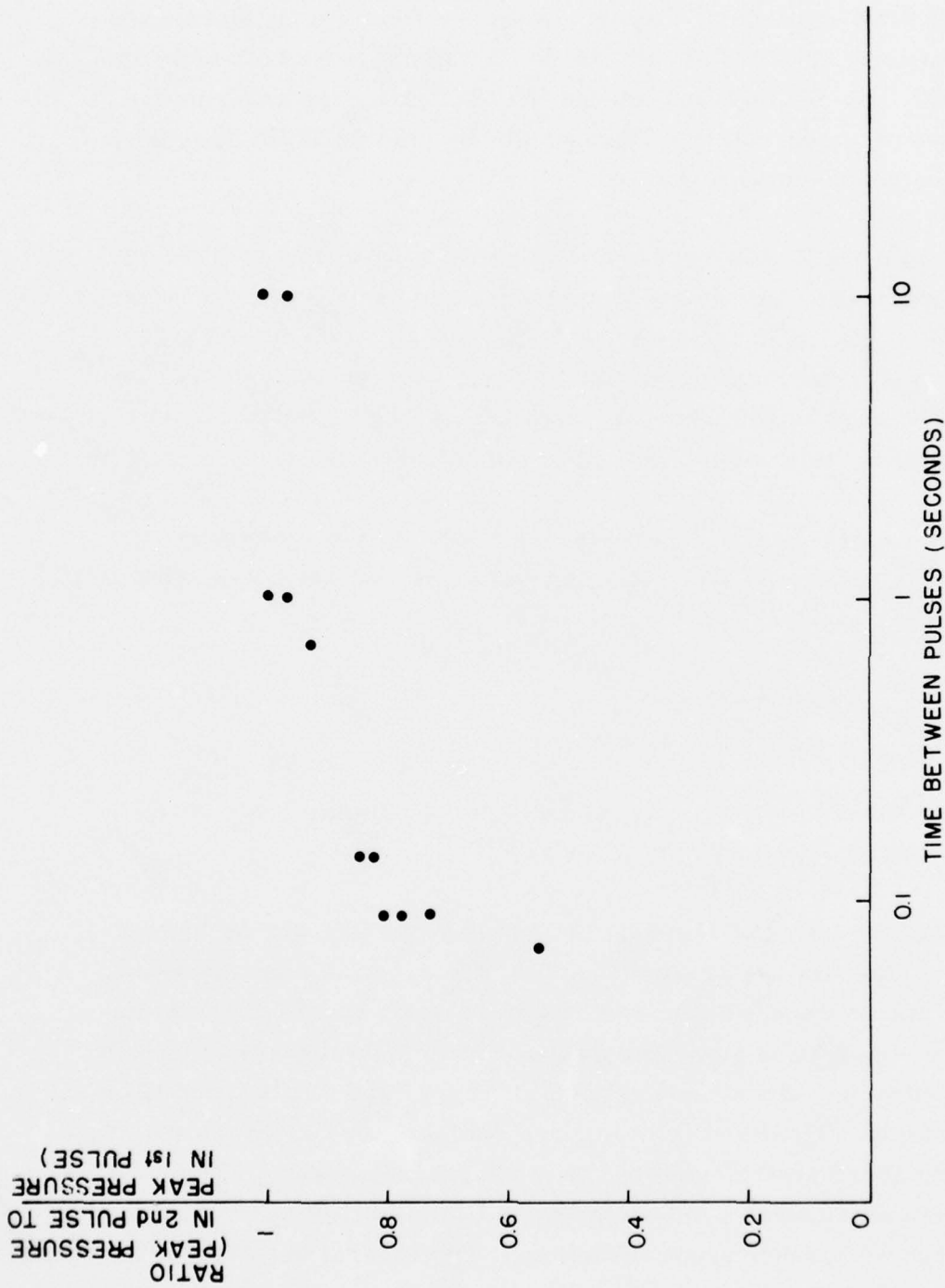


Figure II-8. Ratio of the peak shock pressure delivered by the second pulse in a series of two pulses to the peak shock pressure delivered by the first pulse, as a function of interpulse time. The data are relevant to a titanium target irradiated at  $1.42 \times 10^8 \text{ w/cm}^2$ .

the interpulse time would be desirable, since the effect was still changing rapidly at our lower limit. This will be one of the prime objectives in our continued work. We will obtain a second CO<sub>2</sub> TEA laser on loan and will pulse the two lasers separately. Thus we will be able to obtain interpulse times in the submillisecond region.

The results in Figure II-8 are somewhat difficult to reconcile with the results of other workers, who measured the total impulse delivered to lead targets by two laser pulses in sequence<sup>(7)</sup>. In this work, a maximum in the total impulse was observed at an interpulse time between 10<sup>-5</sup> and 10<sup>-4</sup> seconds. The resolution of this apparent discrepancy must await the extension of our work into the time regime less than one millisecond.

According to one treatment of laser-induced shock<sup>(8)</sup>, the shock pressure should vary with the nature of the ambient gas. The variation was predicted to be of the form:

$$P \propto \frac{\gamma+1}{2\gamma}^{\frac{2}{\gamma-1}} \frac{(\gamma-1)^{2/3}}{(\gamma+1)^{4/3}} \rho^{1/3}$$

where P is the shock pressure,  $\gamma$  is the ratio of the specific heats of the particular gas and  $\rho$  is the density of the gas.

We investigated the effect of changing the ambient gas to argon or helium, instead of air. Results are presented in Table II-2. This table presents data for the ratio of the peak pressure observed in the specified gas to the peak pressure observed in air. The first column lists the gases for which the ratio is relevant. The second column gives the values calculated from the above equation. The third column gives the measured value for the ratios. All numbers are relevant to one atmosphere pressure. The observed results were obtained by evacuating the bell jar and then backfilling to one atmosphere with either argon or helium. The general variation of the ratio with the ambient gas is as expected, although the observed values are somewhat lower than the calculated values.

Table II-2. Ratios of Peak Pressures for Irradiation  
in Different Ambient Gases

	Expected Value	Observed Value
Ar/Air	1.30	1.19
He/Air	0.604	0.45

In comparing these results on shock pressure to earlier results<sup>(2)</sup> on impulse, we find a reasonable consistency in the orders of magnitude. In the work presented here, at one atmosphere ambient pressure, the peak shock pressure is about  $10^8$  dynes/cm<sup>2</sup>, lasting about 3  $\mu$ s, over an area of around 0.01cm<sup>2</sup>. On this basis one would expect a total impulse around 3 dyne-second, in reasonable agreement with the approximate values around 5 dyne-second obtained earlier for total impulse. In vacuum (<10 torr), we observed a peak shock pressure around  $10^7$  dyne/cm<sup>2</sup>, lasting about 3  $\mu$ s, over an area of around 0.01 cm<sup>2</sup>, leading to an expected impulse around 0.3 dyne-second. This compares well with the value of 0.4 dyne-second observed at pressures below 10 torr.

Because of great interest in alkali halide laser window materials, and because of the importance of high resistance to damage for these windows, we measured laser-induced shock pressure in potassium chloride, a leading candidate for laser windows. Potassium chloride is nominally transparent at 10.6  $\mu$ m, but it is subject to catastrophic damage when the laser power density becomes high. We found a correlation between damage threshold and shock pressure.

To obtain data with this transparent material, the rear surface of the target was polished and vacuum coated with gold to form the mirror in the interferometer. Data on the measured pressure as a function of time for a potassium chloride sample irradiated at  $7.15 \times 10^7$  w/cm<sup>2</sup> are shown in Figure II-9. When we compare these results to those obtained with metallic

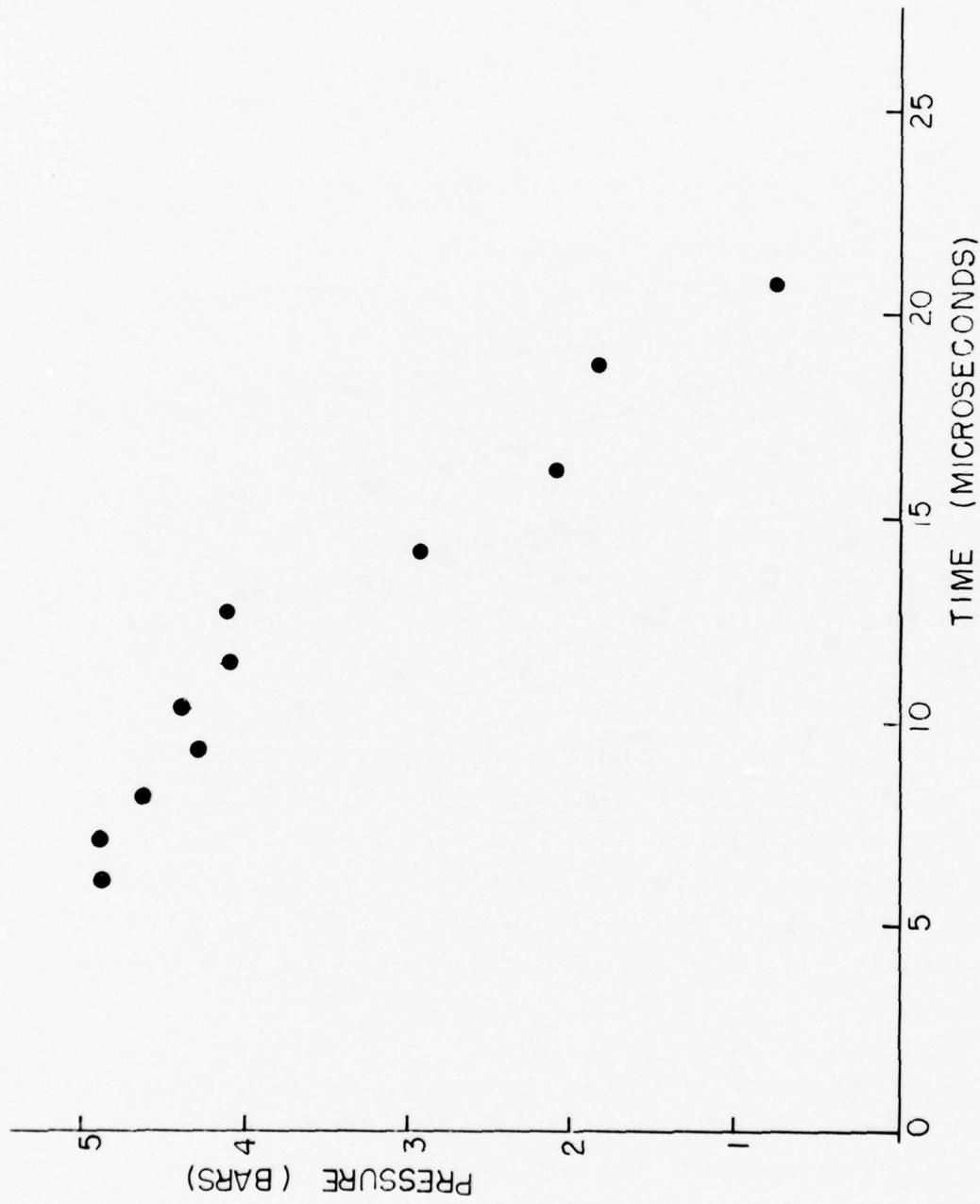


Figure II-9. Shock pressure as a function of time in a potassium chloride target irradiated at  $7.15 \times 10^7 \text{ w/cm}^2$ .

surfaces, we find several differences. For a comparable level of laser power density, the peak shock pressure is considerably lower for potassium chloride. Also, the duration of the shock is longer, by a factor of 5. These differences may be due to differences in elastic properties for the different types of material. The alkali halides are more brittle and more subject to damage by fracture than are metals. When the material fractures, the amount of energy dissipated in producing the fracture is no longer available for the propagating shock front. The finite time for fracture and possibly greater dispersion for the shock velocity may account for the longer temporal duration in potassium chloride.

Figure II-10 illustrates the power dependence of the shock in potassium chloride. There is a threshold around  $4 \times 10^7 \text{ w/cm}^2$ , below which the shock pressure decreases to a very low value. This threshold value for producing a shock coincides with the threshold for igniting a visible spark on the surface. Thus when the laser-supported absorption wave is ignited, the pressure that it transmits into the material is high enough to cause damage by fracture.

Photographs of the damage produced on the surface of potassium chloride targets are shown in Figures II-11, II-12 and II-13. Figure II-11 shows damage observed near threshold. This threshold damage takes the form of cracking along the surface, along with small surface pits, presumably at the sites of surface imperfections. The cracks are initiated at the small sites of material removal.

Figure II-12 shows heavy damage and material removal at a level well above threshold. The damage takes the form of a pit with boundaries formed by crystalline cleavage planes. This implies that laser-produced shocks produce fracture along crystalline planes, followed by expulsion of the resulting rubble.

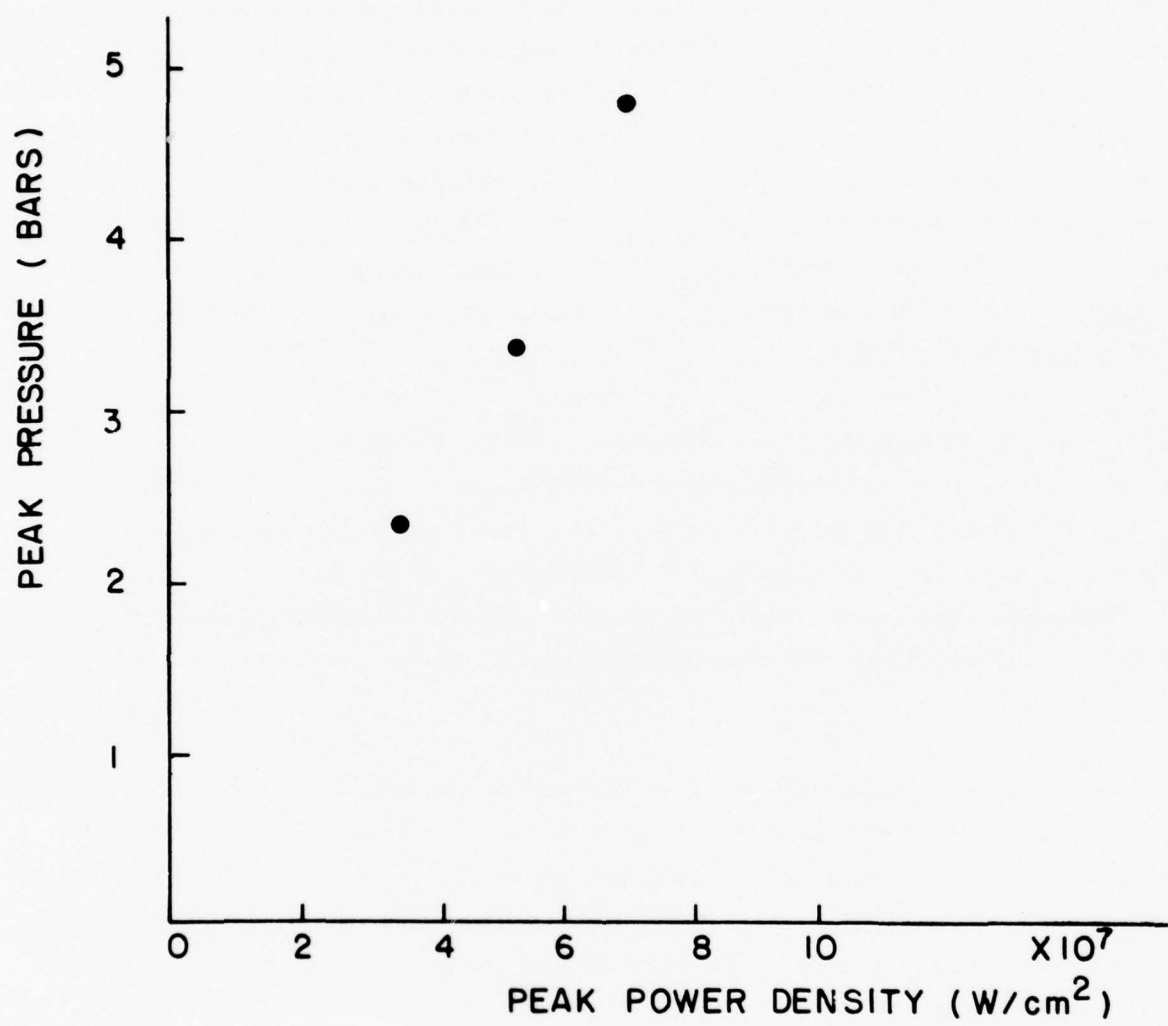


Figure II-10. Peak shock pressure as a function of laser power density for potassium chloride.

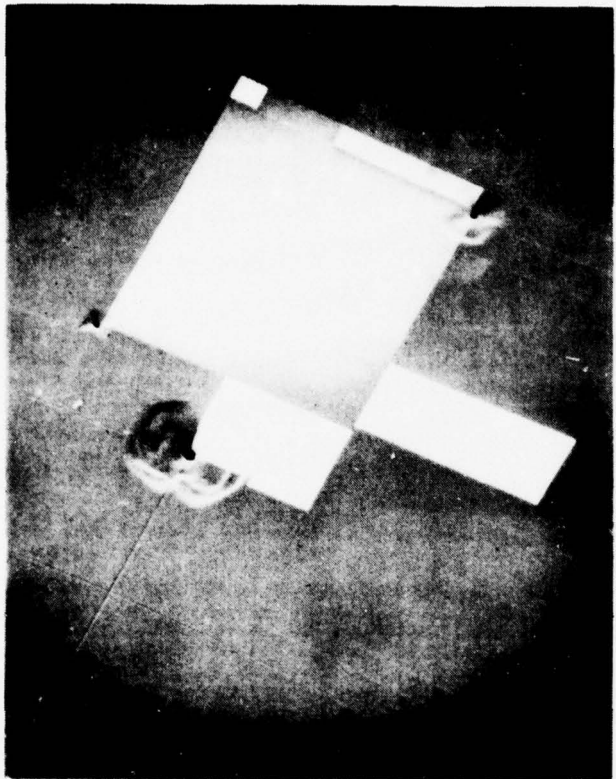


Figure II-11. Scanning electron microscope photograph of threshold damage in a potassium chloride target. Magnification is 100X.

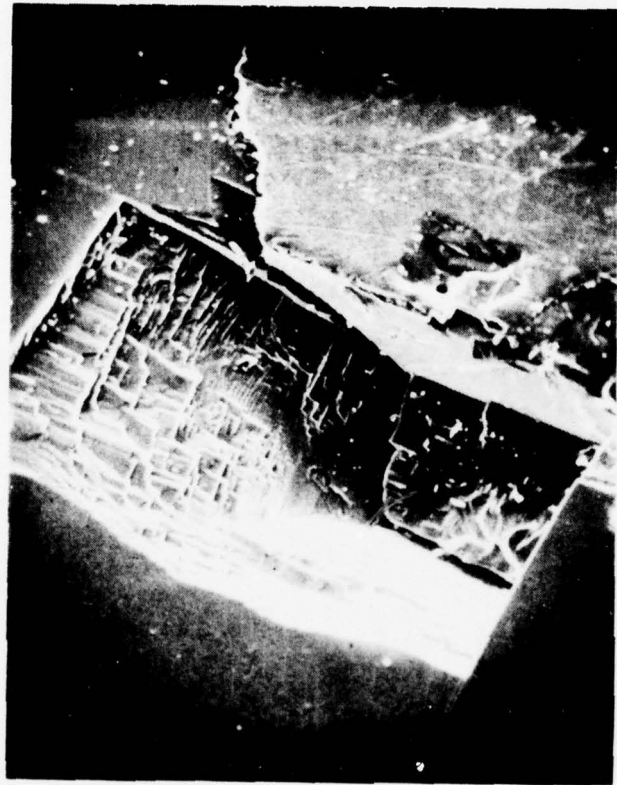


Figure II-12. Scanning electron microscope photograph of a pit produced by impact of a laser pulse at a level well above the threshold for damage on a potassium chloride surface. Magnification is 200X.



Figure II-13. Scanning electron microscope photograph of details of the damage produced by the impact of a laser pulse well above the threshold for damage on a potassium chloride target. Magnification is 500X.

Figure II-13 shows more detail for a heavily damaged region, giving a clear view of the sharp edges and complicated patterns of cracking and material removal.

We mentioned above that the threshold for surface damage of a potassium chloride sample with a gold-coated rear surface was around  $4 \times 10^7 \text{ W/cm}^2$ . This is a value lower than that observed on samples with no coating. We investigated this discrepancy, with results as presented in Table II-3. The first column of numbers gives results observed for damage threshold in potassium chloride samples with no coating on the rear surface. The next column gives results when there is a gold coating. These numbers are the values for threshold specified in terms of the raw incident laser power density. They are systematically lower than those in the first column, by more than the experimental uncertainty, which is around 10 percent. We considered the possibility that light reflected from the gold-coated rear surface adds to the incident light, so as to increase the effective power density. The beam is focussed near the front surface. The beam diverges from its focus, travels through the sample, is reflected from the rear surface, and traverses the sample again. The resultant power density at the front surface due to this reflection may be derived from simple geometrical considerations. This value was added to the incident value to obtain a corrected effective power density at the front surface. The numerical results are presented in the final column of Table II-3. They agree reasonably well with the numbers in the first column, within our experimental uncertainty of 10 percent. Thus the apparently anomalous result of decreased damage threshold when the rear surface is gold-coated can be interpreted simply. It results from an increase of effective power density through light reflected from the coating.

Table II-3. Threshold for Front Surface Damage on KC1

	No Coating on Rear Surface	Au Coating on Rear Surface	Au Coating on Rear Surface (corrected)
First Shot at Full Power	$5.5 \times 10^7 \text{ w/cm}^2$	$3.6 \times 10^7 \text{ w/cm}^2$	$5.9 \times 10^7 \text{ w/cm}^2$
With Pre- Conditioning at Lower Power	$1.2 \times 10^8 \text{ w/cm}^2$	$6.4 \times 10^{7*} \text{ w/cm}^2$	$9.8 \times 10^{7*} \text{ w/cm}^2$

\*Au coating partially removed during preconditioning

We also studied the effect of preconditioning the potassium chloride surface at lower values of laser power density. Other workers have found that this technique increases the damage threshold<sup>(9)</sup>.

The technique involves firing the laser a number of times at the surface, at values below the damage threshold. The power is increased gradually, until the damage threshold is reached. The values obtained in this way exceed values found when the first pulse on an area is at full power.

Our measured results are shown in the bottom row of Table II-3. The effect is clearly demonstrated. These results agree with the results of the other investigators<sup>(9)</sup>. Also, note that when we preconditioned a target with a gold coating, the gold coating was partially damaged. These results, marked with an asterisk, must be considered as less certain than the other values.

These results are consistent with the phenomenology obtained from Figure II-11, which shows that fracture begins at the sites of impurities. If the impurities can be removed at relatively low power density, without producing a shock front which will fracture the material, the damage threshold increases markedly.

These results are of considerable interest, because of the importance of alkali halide materials as windows for high power lasers. The damage mechanism for failure of the windows at high laser power densities is demonstrated and techniques for improving the damage threshold are demonstrated.

The results described in this section have been accepted for presentation at the 1977 IEEE/OSA Conference on Laser Engineering and Applications, Washington, D. C., June 1-3, 1977.

### SECTION III SURFACE CHARACTERIZATION

We have used two different techniques to characterize the metallic surfaces of our target materials. It is important to do this so that we can effectively evaluate the role played by the particular surface in producing the observed results. The two techniques employed were (1) Auger spectroscopy and (2) (2) scattered light measurement to obtain the spectral density function characteristic of the surface.

Auger spectroscopy was carried out with a Physical Electronics Corporation Auger microprobe, located at the University of Minnesota in Minneapolis. This equipment is available for rental. Figures III-1, III-2 and III-3 show profiles for stainless steel target surfaces. Figure III-1 is for an unirradiated target surface. Figure III-2 is for a stainless steel surface irradiated in vacuum (less than one torr) and Figure III-3 is for a surface irradiated in air. The presence of an oxygen layer on the surface is apparent. The origin of this layer is uncertain, because the samples had been exposed to air between irradiation and Auger analysis. Nevertheless the sample irradiated in air showed considerably more oxygen, extending to a greater depth, than the other samples. The differences are sufficiently great to infer that this is caused by oxidation of the surface during the period that it is hot following the laser irradiation.

Data on the estimated compositions of the stainless steel targets as a function of depth are given in Table III-1. These results are obtained from the Auger analysis. Although Auger spectroscopy is not a completely quantitative technique, the results at depths of a few hundred angstrom units are in reasonable agreement with nominal values for the different constituents. This implies that the numerical values in Table III-1 can be interpreted as reasonably accurate, at least for the major constituents. At a depth of approximately  $400\text{\AA}$  units, the material has composition similar to the nominal composition and oxygen has decreased to a few percent.

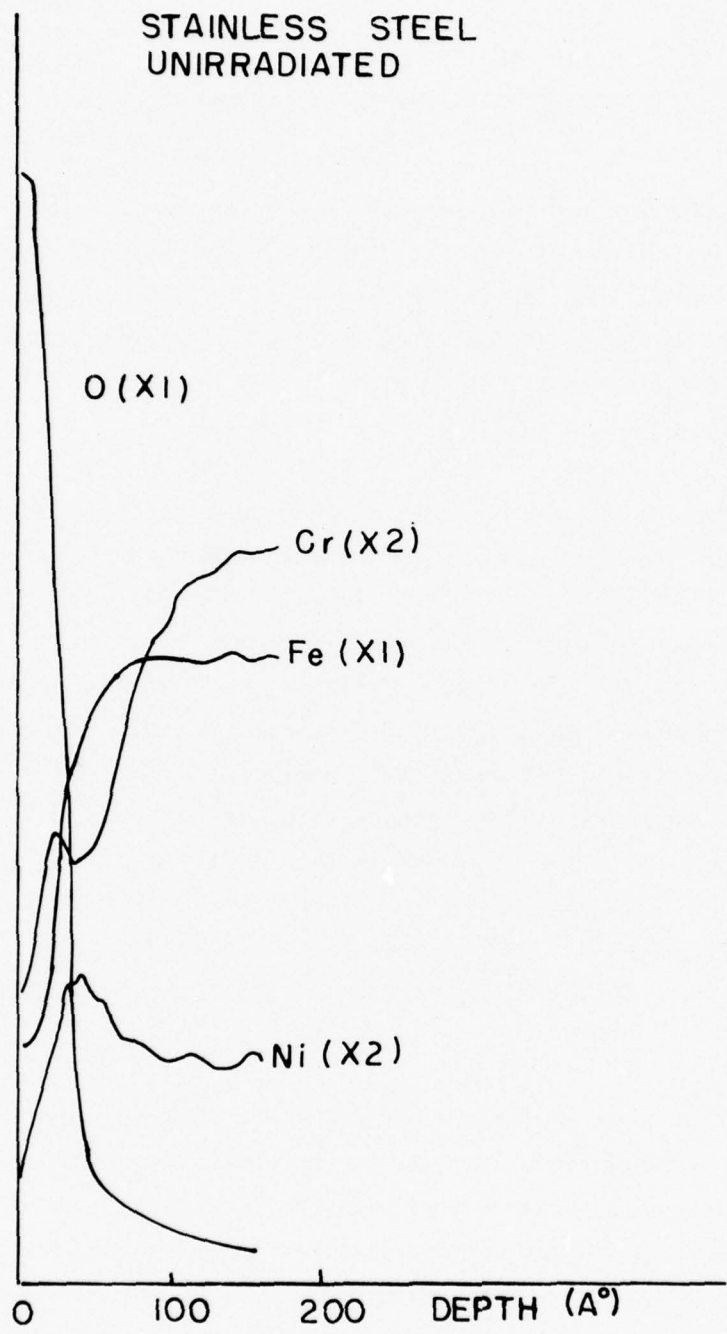


Figure III-1. Composition as a function of depth for a stainless steel target as obtained by Auger spectroscopy. The target had not been laser irradiated. The vertical scale is arbitrary.

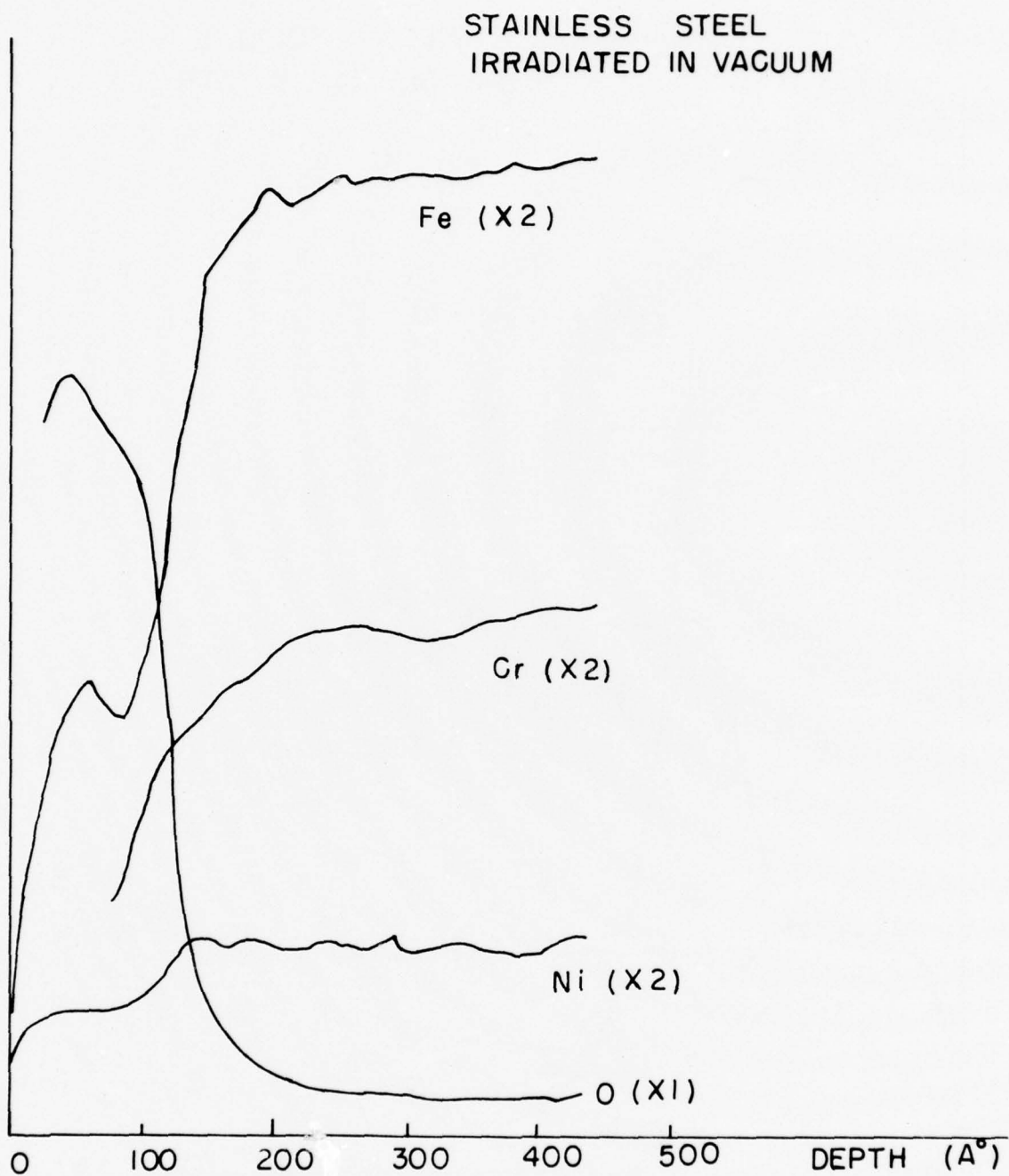


Figure III-2. Composition as a function of depth for a stainless steel target as obtained by Auger spectroscopy. The target had been laser irradiated in vacuum. The vertical scale is arbitrary.

STAINLESS STEEL  
IRRADIATED IN AIR

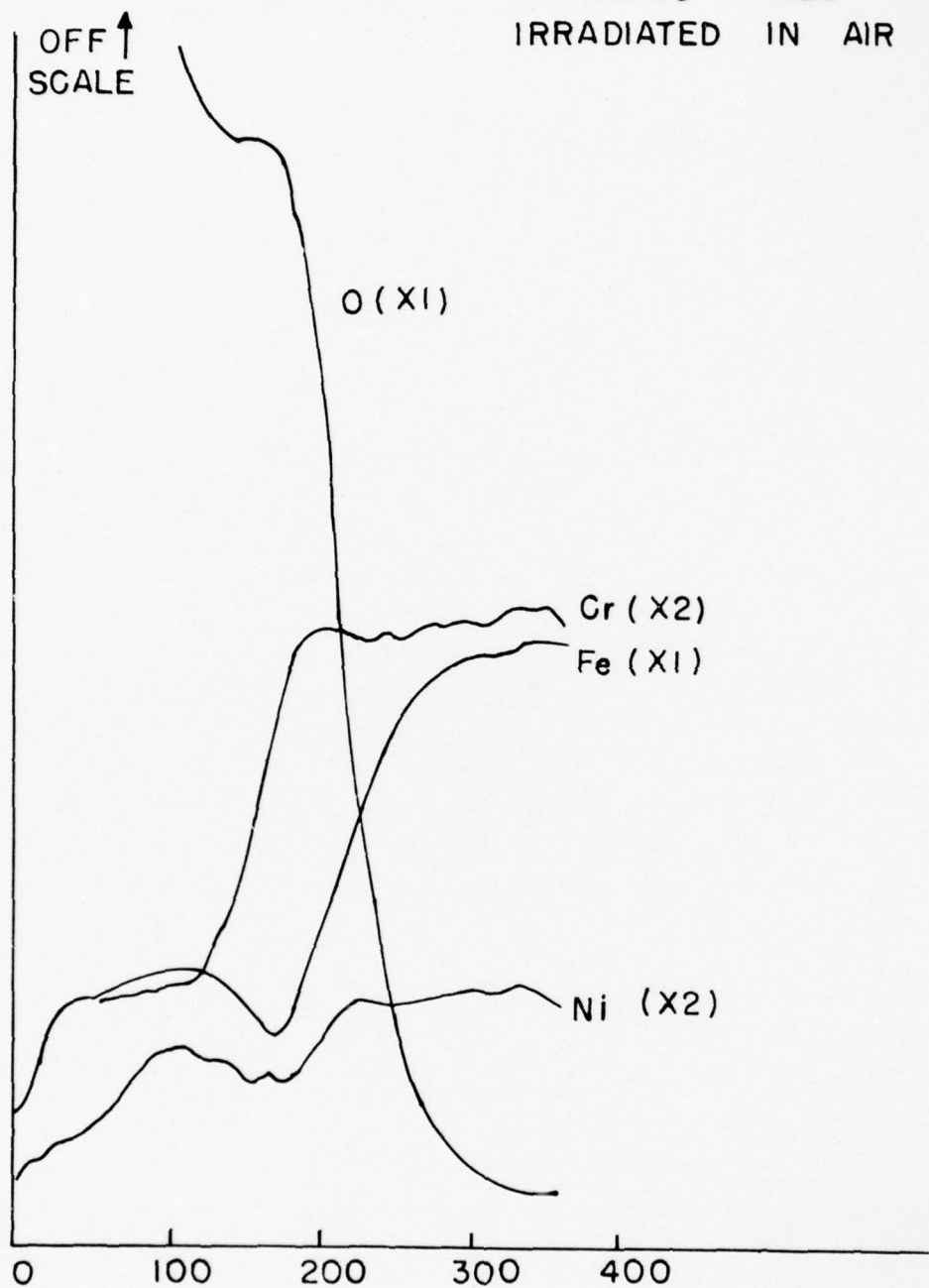


Figure III-3. Composition as a function of depth for a stainless steel target as obtained by Auger spectroscopy. The target had been laser irradiated in air. The vertical scale is arbitrary.

Table III-1. Compositions (percent) for Stainless Steel Targets

	<u>Unirradiated</u>	<u>Irradiated in Vacuum</u>		<u>Irradiated in Air</u>		<u>Nominal</u>
Depth ( $\text{\AA}$ )	0	167	0	438	0	371
Fe	25	69	14	66	13	~70
Cr	7	20	6	18	3	17-19
Ni	4.5	7.5	2.5	7.5	2	8-10
C	7	1.5	35	3.5	25	<0.15
O	38	1	12	3	Off Scale	~0
Al	4	~0	~0	~0	~0	~0

One important conclusion is that aluminum is present on the outer surface of the unirradiated samples. It is not detectable on the surface of samples irradiated either in vacuum or in air. It is not present at a depth of  $167\text{\AA}$  in the unirradiated sample. This implies that surface polishing, which was carried out with alumina, for samples used in our earlier reflectivity measurements, did leave a film of aluminum oxide on the surface. This film was left as a residue from the polishing and was removed by the irradiation.

To determine if this film plays any role in the measurement of surface reflectivity, we will carry out future measurements with target surfaces prepared in other ways and polished with other compounds. Thus, we will be able to determine the possible effect of the aluminum on the outer surface.

The second technique for surface characterization involves measuring the spectral density function, according to a method proposed by Stover<sup>(10, 11, 12)</sup>. The spectral density function is a mathematical characterization based on the concept of Fourier composition. If the displacement,  $Z$ , of the surface from its mean position is given by  $Z(X)$ , where  $X$  is the transverse coordinate, one may express  $Z(X)$  as a Fourier series:

$$Z(X) = \sum_i a_i \sin(2\pi f_i X + \phi_i)$$

where  $a_i$  and  $\phi_i$  represent the amplitude and phase, respectively, relevant to frequency  $f_i$ . The spectral density function, then, is proportional to  $a^2$ .

Measurements of the laser light diffusely scattered from the surface as a function of scattering angle can be used to measure the spectral density function. A schematic diagram of the apparatus used for this measurement is shown in Figure III-4. Light is incident on the surface at an angle  $\alpha$  from the surface normal. The scattered light is measured as a function of the angle  $\theta$ , by rotating a detector so as to vary  $\theta$ . The spectral density function is given by:

$$a^2(\theta) = \frac{P_1(\theta) \lambda^2}{4\pi^2 P_0 \cos \theta \cos \alpha}.$$

where  $P_1$  is the detected power measured at angle  $\theta$ ,  $P_0$  is the power measured at the specular angle and  $\lambda$  is the wavelength of the light.

We set up apparatus as shown in Figure III-4 and measured the scattered light as a function of angle for surfaces of interest. Different types of surfaces having different histories showed characteristically different signatures when the spectral density function was plotted as a function of frequency. This is shown in Figure III-5. Unirradiated surfaces show functions which have a peak at the spatial frequency corresponding to the inverse of the diameter of the polishing grit. This accounts for the peak which is becoming apparent at a spatial frequency of 1.6 inverse micrometers. This was the maximum spatial frequency which could be probed with the helium-neon laser of wavelength 0.6328 micrometers. (Using a helium-cadmium laser would have allowed measurements to a higher spatial frequency.) On laser-irradiated surfaces this peak has been suppressed, indicating that laser-induced melting has smoothed small scratches produced by the polishing. An unirradiated area with vertical scratches shows a pronounced peak near 1.4 inverse micrometers, due to the scratches.

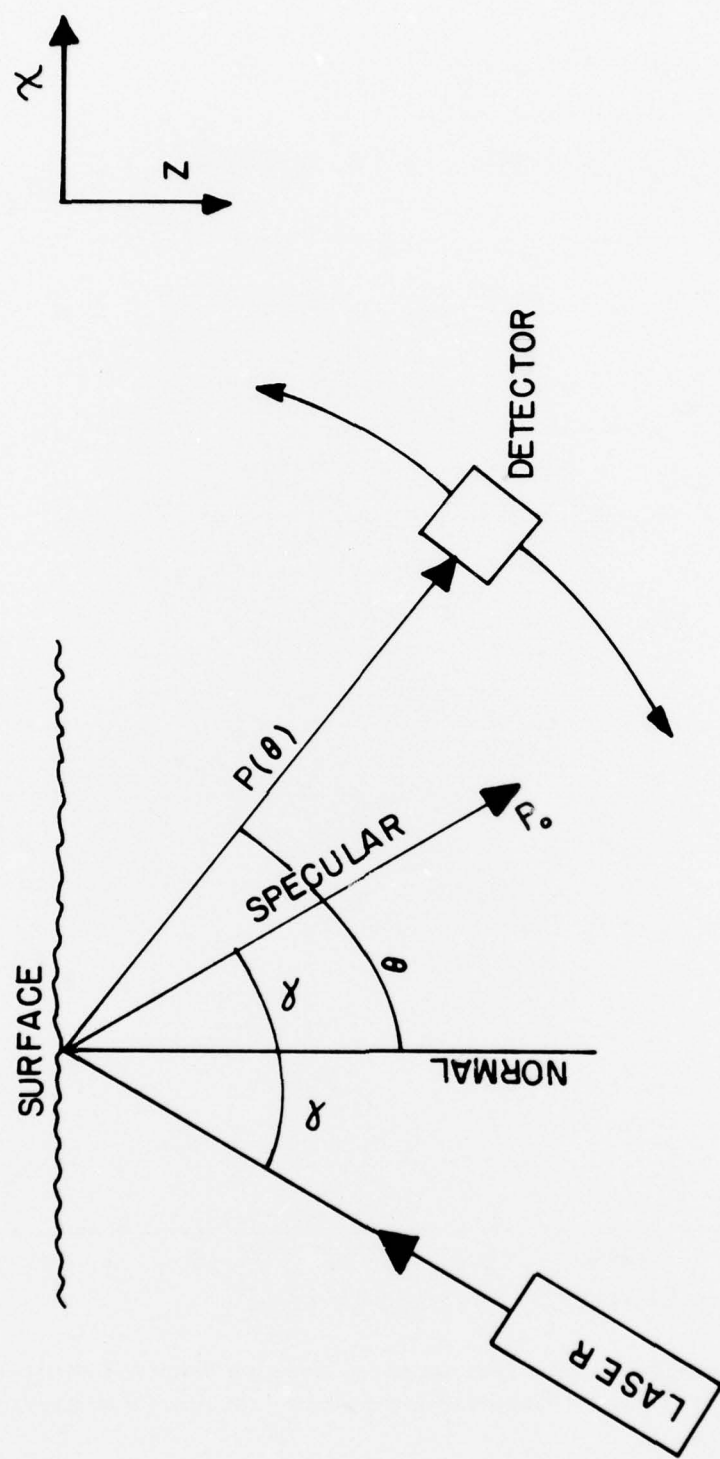


Figure III-4. Experimental arrangement for measurement of spectral density function.

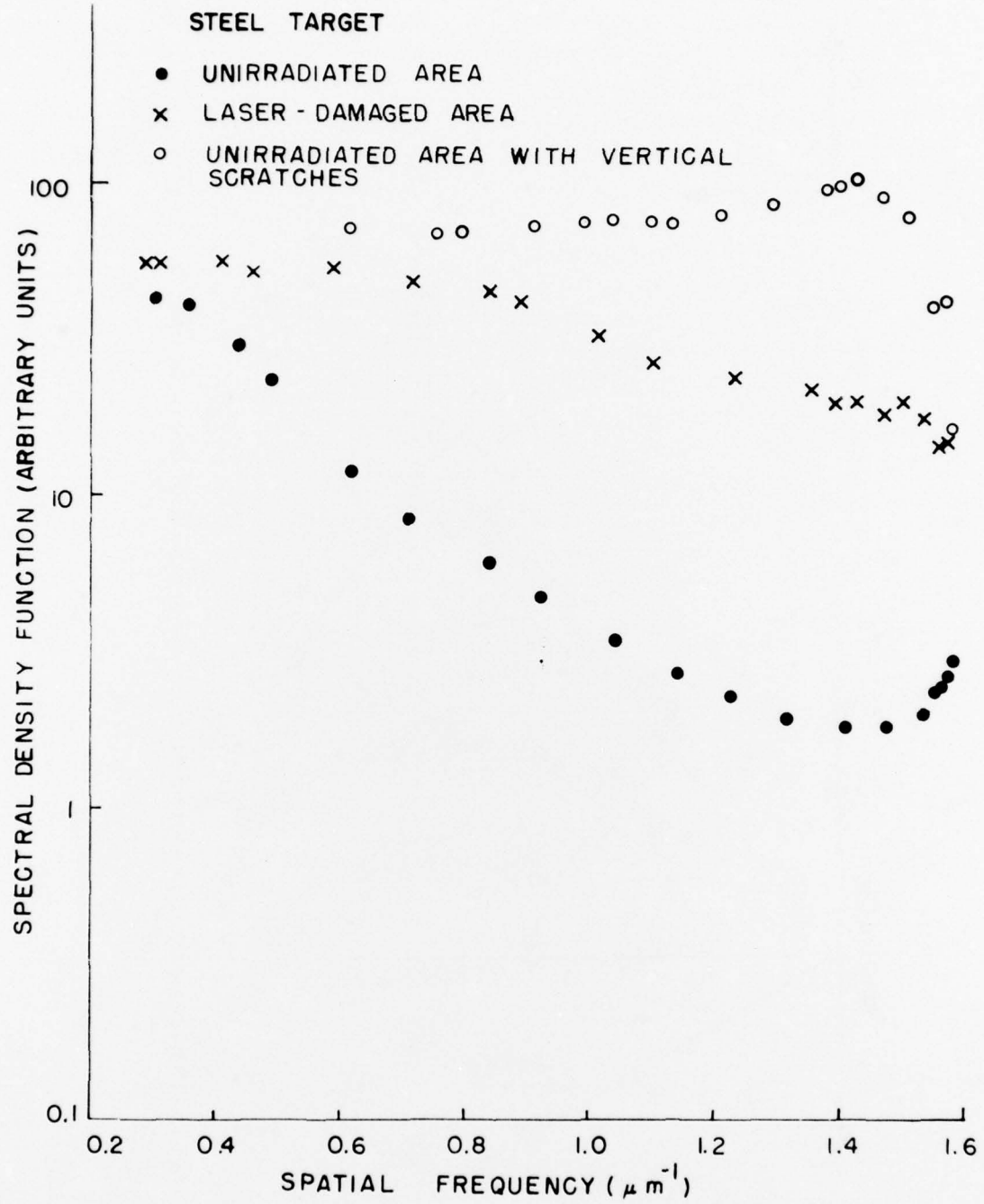


Figure III-5. Measured values for spectral density function (normalized) as a function of spatial frequency, for various surfaces.

The melting and flow of the material induced by the laser radiation produces surfaces with irregularities with a scale around 2 to 3 micrometers<sup>(2)</sup>. This increases the scattering of helium-neon laser light relative to that of the longer wavelength CO<sub>2</sub> laser light. Thus, our reflectivity measurements indicate that the reflectivity decreases more strongly for visible light than for CO<sub>2</sub> laser light. This is consistent with the measurements in Figure III-5, where the laser-irradiated surface shows a relatively high value of the spectral density function at a spatial frequency of less than 1 inverse micrometer.

In summary, measuring the spectral density function of the scattered light has proven to be a valuable tool for probing the characteristics of the target surfaces.

## SECTION IV COUPLING OF LASER ENERGY TO BLOWOFF MATERIAL

In a previous report<sup>(3)</sup> we described measurements of the coupling of laser energy to the laser-produced blowoff material, as derived from measurements in our time-of-flight mass spectrometer. Data were presented for the distribution of energy in the various degrees of freedom in the blowoff material, including the kinetic energy of expansion, the heat of vaporization required to produce the observed amount of blowoff material, and the amount of energy needed to produce the observed mixture of ionization states. The fraction of the total laser energy coupled into the blowoff was 6 percent when the laser was operated with nitrogen on and 4.2 percent when the laser was operated with nitrogen off. We have now obtained data giving the variation of these numbers with laser power density. These data are presented in Figure IV-1, which gives the fraction of the incident laser energy carried away by the blowoff as a function of laser power density, for an aluminum target. The fraction is higher for the longer pulse, implying that absorption in the blowoff material continues during the lower power tail of the pulse. These results show that even for the low ambient air pressures in the time-of-flight mass spectrometer, there is a significant absorption of laser energy in the blowoff material. The fraction of the total energy absorbed in the blowoff material is consistent with values measured for transmission of the blowoff material at low ambient air pressure<sup>(3)</sup>.

Thus, we have obtained values for the energy required to produce the blowoff material in its observed state. We have found that the largest contributor is the kinetic energy of expansion, and that the total amount of energy is just a few percent of the energy delivered by the laser. Some fraction of the energy remains within the sample as thermal energy which increases the sample temperature, and the remainder is reflected, either diffusely or specularly. These measurements are important for determining the total partition of the energy delivered by the laser to the target surface.

These results have been submitted for publication to Applied Physics Letters.

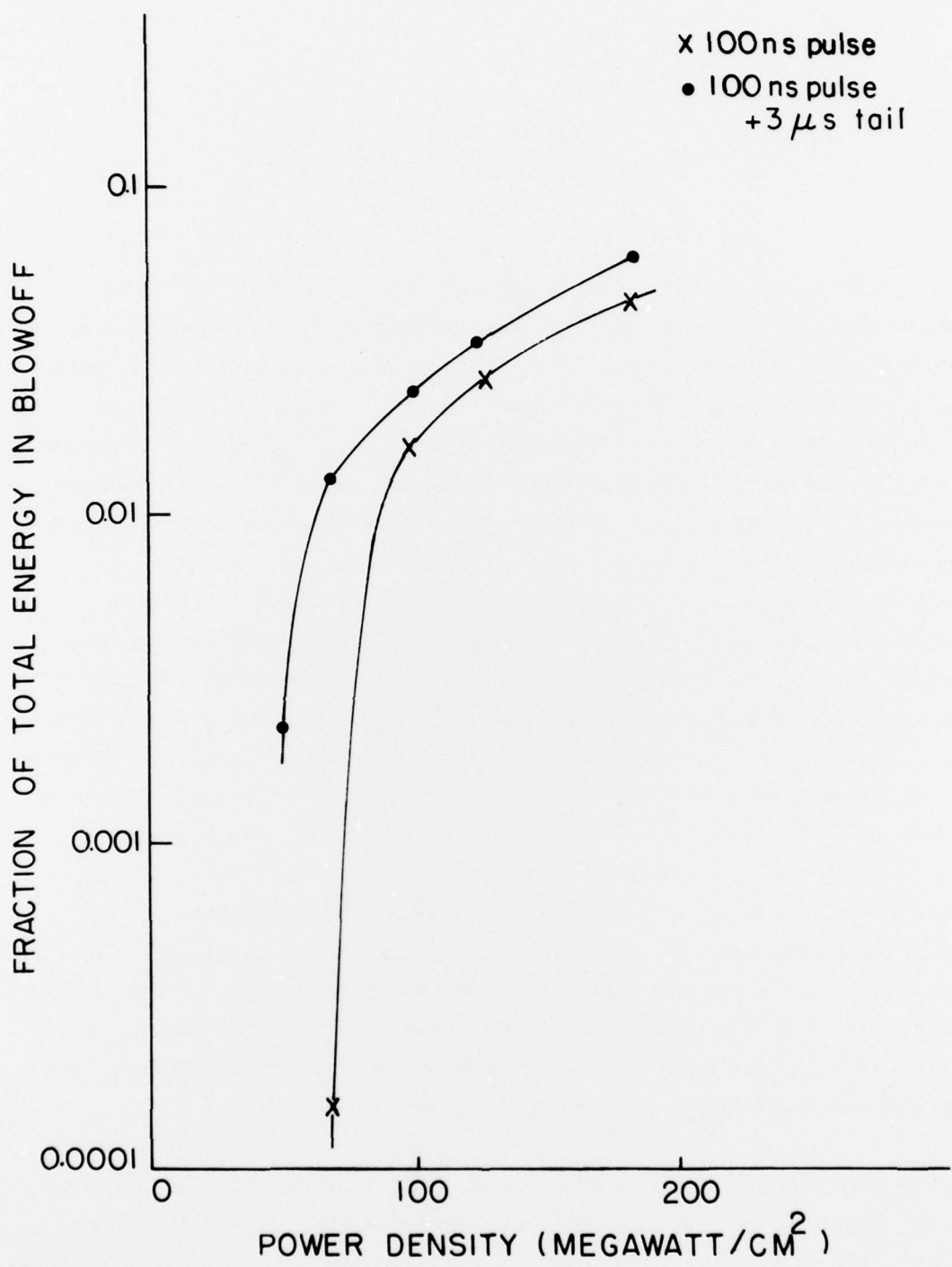


Figure IV-1. Fraction of incident laser energy carried away by blowoff material, as a function of laser power density.

## SECTION V REFLECTIVITY

Only one measurement relative to the effect of laser irradiation on target reflectivity was performed during this contract period. This consisted of measuring the change in specular reflectivity produced by two pulses, with variable interpulse times. These measurements were taken relative to the permanent change in specular reflectivity produced by the laser irradiation. They were measured by the method described previously<sup>(2)</sup> using a helium-neon laser as a probing beam. Measurements were carried out in ambient air under conditions where the specular reflectivity at  $0.6328 \mu\text{m}$  was considerably reduced by one single laser shot. The results are shown in Figure V-1. What is presented is the specular reflectivity after a series of two laser shots at the indicated interpulse time. The results are normalized to the initial value as unity. For a laser power density of  $1.2 \times 10^8 \text{ w/cm}^2$ , the reflectivity is reduced to around 15 percent of its pre-irradiation value by the series of two shots. Thus, each data point represents the final reflectivity after the two shots have been delivered. The data have some scatter, but indicate no systematic dependence of the final reflectivity on interpulse time, down to approximately 20 milliseconds. This result is difficult to reconcile with the result shown in Figure II-8, in which significant effects were observed for interpulse times of 70 milliseconds. If the earlier results (Figure II-8) are caused by absorption of laser light in blowoff material remaining from the first shot, it is difficult to understand the independence of the final reflectivity on interpulse time.

The minimum interpulse time of 20 milliseconds could be obtained only on a few shots. Most of the data was taken at interpulse times of 80 milliseconds or greater. When the data in Figure II-8 were obtained, we could not produce pairs of pulses of equal amplitude with an interpulse time of less than 70 milliseconds. As with the other data, only pairs of pulses of equal amplitude were accepted.

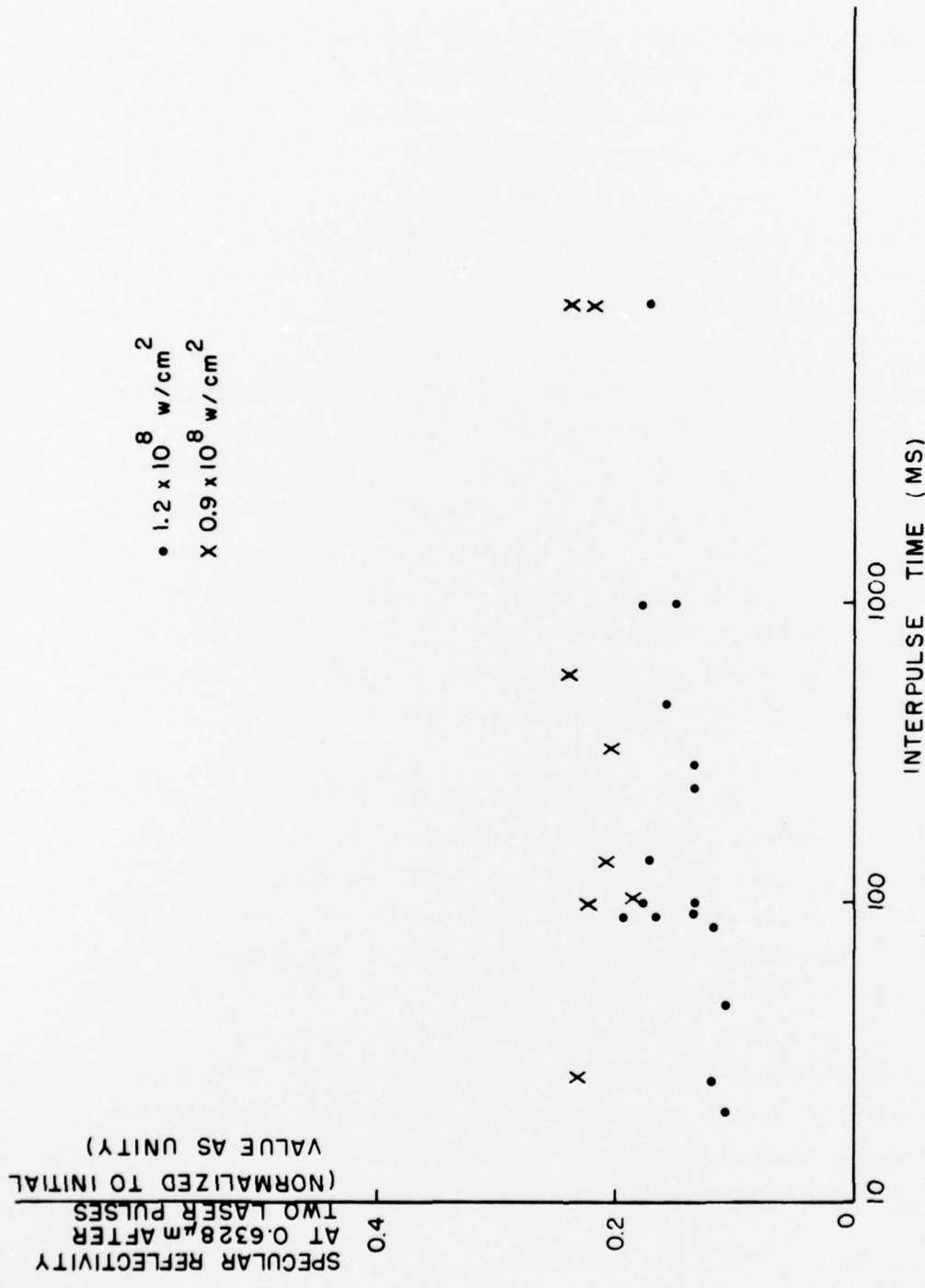


Figure V-1. Specular reflectivity at  $0.6328\mu\text{m}$  after impact of two successive laser pulses on a stainless steel target, as a function of interpulse time.

Continued work in this area will involve using two TEA lasers which can be pulsed independently at times variable down into the microsecond regime. We anticipate that the apparent discrepancy between Figure V-1 and Figure II-8 can be resolved with more measurements at shorter interpulse times.

Our previous results on measurements of time-resolved reflectivity have led us to a simple method of extending the measurements on specular reflectivity to include both specular reflectivity and diffuse reflectivity measurements. We noted that non-time-resolved measurements of specular and diffuse reflectivity and absorptivity after the end of the laser pulse added to unity.<sup>(2)</sup> This, of course, is true throughout the pulse but the conclusion is that our measuring techniques have sufficient credibility to measure two of the three parameters on a time-resolved basis and to derive the third by subtraction from unity. Accordingly, we are setting up instrumentation to extend the previous measurements on specular reflectivity. The extension involves using an integrating ellipsoidal mirror. The ellipsoidal mirror collects all the probing light reflected from the target and thus allows time-resolved measurements of total reflectivity.

In this experiment the sample and the detector are placed at two foci of the ellipsoid. As is well known, a light ray passing from one focus of an ellipsoid will reach the other focus regardless of direction of travel. Thus, the profile of the probing beam on the target is re-imaged on the detector. All the diffusely scattered probe radiation reaches the detector, regardless of the direction at which it leaves the target surface. Thus, diffusely reflected radiation can be collected and measured with a high frequency detector. The ellipsoidal mirror has the advantage over a hemispherical mirror of reduced image size and conveniently large spatial separation of sample and detector.<sup>(13)</sup> Separation of components is important for accommodating suitable mounts for the target and the detector.

Small changes in the configuration of this experiment will allow us to measure either specular, total or diffuse reflectivity on a time-resolved basis. The total reflectivity can be measured on a time-resolved basis if the probe beam is incident on the target surface at a small angle from the surface normal. Then the specularly reflected beam will reach the detector, along with diffusely scattered light. If a small opaque beam stop is inserted in front of the detector with a small aperture through which the specularly reflected beam can pass, we can obtain measurements of the specular reflectivity, similar to our earlier results.

If the probe beam strikes the target along the normal to the target surface, specularly reflected light will be directed back out the entrance hole in the ellipse and will not reach the detector. In this configuration the detector will see only diffusely scattered light. Thus, we can measure time-resolved diffuse reflectivity separately during irradiation.

The ellipsoid is cast of aluminum-filled epoxy and has a coating of vacuum-deposited aluminum. The major and minor axes are 24.85 and 23.85 cm, respectively, and the separation between foci is 7 cm. This allows adequate room for mounting the target and detector.

The two laser beams enter the ellipse through a hole in the mirror wall. Knowing the size of the image is important, because the entrance aperture of the detector must be large enough to admit all the image flux. For an ellipsoid, the magnification is fixed by the length of the semi-major axis and the separation of the foci. By keeping the irradiated area on the target small and centered on one focus, the image size is small and collection loss is minimized. Image sizes of the order of 1 millimeter can be obtained.<sup>(13)</sup>

Calibration is needed to establish the magnitude of flux loss from the ellipsoid. Losses can be expected from flux being reflected out the entrance hole and from absorption in scattering at the mirror surface. The mirror

efficiency usefully expresses the loss. Efficiency is the ratio of detected signal with and without the ellipsoid. The signal with the ellipsoid is obtained by bringing flux into a standard reflection target at one focus while the detector is at the other focus. The signal without the ellipsoid is measured by removing the standard target and placing the detector in the target position. The ratio of signals so obtained is unity for a perfect ellipsoid and less than unity for a real ellipsoid.

Calibration is also possible by comparison with static values for total specular and diffuse reflectivity for the same surfaces. These quantities can be determined by the methods used in previous measurements, that is, integrating spheres and calorimetric methods.

To be able to carry out measurements as a function of ambient air pressure, a vacuum station has been constructed for the ellipsoid. A bell jar will completely contain the ellipsoid, target and detector. The target mount will allow remote movement of a target through a vacuum bellows assembly, so that a new area on the target can be presented for successive laser shots.

Measurements with this apparatus will allow us to obtain the time-resolved coupling of laser energy into the target surface. The construction of the apparatus has been completed and we anticipate that initial measurements using this system will be carried out in the near future.

## SECTION VI

### CONCLUSION AND FUTURE PLANS

This report has described several experimental accomplishments, in which we have used a pulsed CO<sub>2</sub> TEA laser to gather data on the interaction of high power laser radiation with target materials.

Much of the report has been concerned with measuring the pressure pulse coupled into the target. Specific results are:

- New data on laser-induced pressure as a function of conditions of irradiation
- Support of a previously developed model by the experimental data
- Identification of the role of the laser-supported absorption wave in transmitting shock pressure to solid targets
- Quantitative results for shock pressures in alkali halide window materials
- Relation between shock pressure and damage in alkali halides

In addition, we have described new results related to characterization of target surfaces by Auger spectroscopy and by surface scattering measurements. We have determined the fraction of incident laser energy coupled into the blowoff material, as a function of laser power density.

Some unresolved issues remain to be dealt with in future work. The effect of variable interpulse time on our results is a prime remaining issue, as described in Section II.

Our future plans include the following items:

- Measuring diffuse reflectivity and specular reflectivity as a function of time during irradiation, using the integrating ellipsoid described in Section V. These measurements will be carried out as a function of ambient air pressure, laser power density, probing laser wavelength and interpulse time. We will use the results to obtain the absorptivity as a function of time and thus to derive the laser power actually absorbed by the target surface as a function of time.
- We will extend the measurements on enhanced thermal coupling by borrowing a second TEA laser and measuring the effect of two successive laser pulses as a function of interpulse time in time regime of tens of microseconds.
- We will carry out measurements on carefully characterized target surfaces prepared by different techniques in order to determine the influence of surface characteristics on the observed results. The characterization will employ the techniques described in Section III. The effect of target surface oxidation will also be investigated. This will be carried out by irradiating targets in a furnace, with the samples being held at elevated temperatures for varying lengths of time prior to irradiation. The amount of oxidation will be monitored by Auger spectroscopy.

## REFERENCES

1. Investigation of Material Damage, Interactions of TEA Laser Radiation with Surfaces, J.F. Ready, Interim Report on Contract F44620-73-C-0022, Covering period from 15 December 1972 to 14 December 1973 (February 1974).
2. Investigation of Material Damage, Interactions of TEA Laser Radiation with Surfaces, J.F. Ready, Interim Report on Contract F44620-73-C-0022, covering period from 15 December 1973 to 14 December 1974 (February 1975)
3. Investigation of Material Damage, Pressure Pulses Produced by Carbon Dioxide Laser Radiation, J.F. Ready, Interim Report on Contract F44620-73-C-0022, covering period from 15 December 1974 to 14 December 1975 (February 1976).
4. J.F. Ready, Applied Physics Letters 25, 558 (1974).
5. J.F. Ready, IEEE Journal of Quantum Electronics QE-12, 137 (1976).
6. E. Bernal G. and J.F. Ready, Journal of Applied Physics 45, 2980 (1974).
7. W.E. Maher and R.B. Hall, Journal of Applied Physics 47, 2486 (1976).
8. R.E. Beverly and C.T. Walters, Journal of Applied Physics 47, 3485 (1976).
9. M. Bass and K.M. Leung, IEEE Journal of Quantum Electronics QE-12, 82 (1976).
10. J.C. Stover, Laser Focus, p. 83 (February 1976)
11. J.C. Stover, in Laser-Induced Damage in Optical Materials: 1974, A.J. Glass and A.H. Guenther, editors, NBS Special Publication 414.
12. J.C. Stover, Applied Optics 14, 1796 (1975).
13. R.P. Heinisch, International Journal of Heat and Mass Transfer 14, 1275 (1971).